Geoscience Frontiers 13 (2022) 101429

HOSTED BY

Contents lists available at ScienceDirect

Geoscience Frontiers

journal homepage: www.elsevier.com/locate/gsf

Research Paper

Recycling process and proto-kimberlite melt metasomatism in the lithosphere-asthenosphere boundary beneath the Amazonian Craton recorded by garnet xenocrysts and mantle xenoliths from the Carolina kimberlite

Fernanda Gervasoni [a,b,*], Tiago Jalowitzki [c], Marcelo Peres Rocha [c], Ricardo Kalikowski Weska [d], Eduardo Novais-Rodrigues [c], Rodrigo Antonio de Freitas Rodrigues [c], Yannick Bussweiler [e], Elisa Soares Rocha Barbosa [f], Jasper Berndt [g], Elton Luiz Dantas [c], Valmir da Silva Souza [c], Stephan Klemme [g]

[a] Centro de Engenharias, Universidade Federal de Pelotas (UFPel), Pelotas, Brazil
[b] Programa de Pós-graduação em Geociências, Universidade Federal do Rio Grande do Sul, Porto Alegre, Brazil
[c] Programa de Pós-graduação em Geologia, Instituto de Geociências, Universidade de Brasília (UnB), Brasília, Brazil
[d] Faculdade de Geociências, Universidade Federal do Mato Grosso (UFMT), Cuiabá, Brazil
[e] Institut für Geologie und Mineralogie, Universität zu Köln, Germany
[f] Faculdade de Ciências e Tecnologia, Universidade Federal de Goiás (UFG), Aparecida de Goiânia, Brazil
[g] Institut für Mineralogie, Universität Münster, Münster, Germany

ARTICLE INFO

Article history:
Received 23 September 2021
Revised 20 May 2022
Accepted 30 June 2022
Available online 05 July 2022
Handling Editor: K. Szilas

Keywords:
Carolina kimberlite
K-rich mantle xenoliths
Ancient subducted slab
Proto-kimberlite melt metasomatism

ABSTRACT

Here we present new data on the major and trace element compositions of silicate and oxide minerals from mantle xenoliths brought to the surface by the Carolina kimberlite, Pimenta Bueno Kimberlitic Field, which is located on the southwestern border of the Amazonian Craton. We also present Sr-Nd isotopic data of garnet xenocrysts and whole-rocks from the Carolina kimberlite. Mantle xenoliths are mainly clinopyroxenites and garnetites. Some of the clinopyroxenites were classified as GPP–PP–PKP (garnet-phlogopite peridotite, phlogopite-peridotite, phlogopite-K-richterite peridotite) suites, and two clinopyroxenites (eclogites) and two garnetites are relicts of an ancient subducted slab. Temperature and pressure estimates yield 855–1102 °C and 3.6–7.0 GPa, respectively. Clinopyroxenes are enriched in light rare earth elements (LREE) (La_N/Yb_N = 5–62; Ce_N/Sm_N = 1–3; where N = primitive mantle normalized values), they have high Ca/Al ratios (10–410), low to medium Ti/Eu ratios (742–2840), and low Zr/Hf ratios (13–26), which suggest they were formed by metasomatic reactions with CO_2-rich silicate melts. Phlogopite with high TiO_2 (>2.0 wt.%), Al_2O_3 (>12.0 wt.%), and FeO_t (5.0–13.0 wt.%) resemble those found in the groundmass of kimberlites, lamproites and lamprophyres. Conversely, phlogopite with low TiO_2 (<1.0 wt.%) and lower Al_2O_3 (<12.0 wt.%) are similar to those present in GPP-PP-PKP, and in MARID (mica-amphibole-rutile-ilmenite-diopside) and PIC (phlogopite-ilmenite-clinopyorxene) xenoliths. The GPP-PP-PKP suite of xenoliths, together with the clinopyroxene and phlogopite major and trace element signatures suggests that an intense proto-kimberlite melt metasomatism occurred in the deep cratonic lithosphere beneath the Amazonian Craton. The Sr-Nd isotopic ratios of pyrope xenocrysts (G3, G9 and G11) from the Carolina kimberlite are characterized by high $^{143}Nd/^{144}Nd$ (0.51287–0.51371) and εNd (+4.55 to +20.85) accompanied with enriched $^{87}Sr/^{86}Sr$ (0.70405–0.71098). These results suggest interaction with a proto-kimberlite melt compositionally similar with worldwide kimberlites. Based on Sr-Nd whole-rock compositions, the Carolina kimberlite has affinity with Group 1 kimberlites. The Sm-Nd isochron age calculated with selected eclogitic garnets yielded an age of 291.9 ± 5.4 Ma (2 σ), which represents the cooling age after the proto-kimberlite melt metasomatism. Therefore, we propose that the lithospheric mantle beneath the Amazonian Craton records the Paleozoic subduction with the attachment of an eclogitic slab into the cratonic mantle (garnetites and eclogites); with a later metasomatic event caused by proto-kimberlite melts shortly before the Carolina kimberlite erupted.

* Corresponding author.
E-mail addresses: fernanda.gervasoni@ufpel.edu.br, gervasoni.fe@gmail.com (F. Gervasoni).

https://doi.org/10.1016/j.gsf.2022.101429
1674-9871/

1. Introduction

Mantle xenoliths are of great scientific importance as they record the mineralogical and chemical changes caused by partial melting and metasomatism. Mantle xenoliths from the subcontinental lithospheric mantle (SCLM) beneath cratons are transported to the surface by kimberlites or similar alkaline volcanic rocks. In kimberlites, it is common to find xenoliths of metasomatized ultramafic rocks, such as mica- and amphibole-rich rocks (Dawson and Smith, 1977; Gregoire et al., 2002), depleted peridotites, and also eclogites (e.g., Aulbach et al., 2007; Pearson et al., 2014 and references therein; Smart et al., 2017). These xenoliths represent direct samples of the cratonic mantle, which is a stratified and heterogeneous part of the upper mantle (e.g., Aulbach et al., 2013), with intense metasomatized portions (e.g., Artemieva et al., 2019), and due to extensive melting, may have depleted and refractory reservoirs (e.g., Walter, 1999; Herzberg, 2004; Ionov et al., 2018).

It is known that the base of the cratonic lithosphere may be strongly reworked and affected by subduction zones and by mantle plumes. For instance, eclogite xenoliths hosted by kimberlites are the products of the oceanic crust subduction into the subcontinental lithospheric mantle (e.g., Aulbach and Stachel, 2022); and mantle plumes are responsible for the lithospheric thinning and posterior recratonization (e.g., Liu et al., 2021). Moreover, the cratonic roots are highly chemically modified by melts or fluids derived from deeper sources that rework and re-enrich the lithospheric mantle (e.g., Menzies et al., 1987; Foley, 1992, 2008). These enrichment processes may change the mineralogy (i.e., modal metasomatism), causing the crystallization of new minerals in the mantle rocks, forming new and metasomatized rock (sometimes veined rocks) composed by hydrous minerals such as micas and amphiboles (e.g., Wass et al., 1980; Foley, 1992, 2008; Konzett et al., 2000). Such metasomatized mantle xenoliths with small amounts of olivine, rich in clinopyroxenes and in hydrous minerals, represent only a small proportion of mantle-derived rocks that are sampled by kimberlites worldwide (e.g., Dawson and Smith, 1977; Nixon, 1987; Gregoire et al., 2002). Nevertheless, these samples are key to unravel the metasomatic processes caused by reactions induced by hydrous alkaline melts and/or fluids within the lithospheric mantle (e.g., Dawson and Smith, 1977; Erlank et al., 1987; Sweeney et al., 1993; Gregoire et al., 2002; Fitzpayne et al., 2018a).

In Brazil, the Carolina kimberlite is part of the Pimenta Bueno Kimberlitic Field that is located on the southwestern border of the Amazonian Craton (Hunt et al., 2009; Weska et al., 2020). This kimberlite hosts a suite of intensely metasomatized mantle xenoliths, which have not been described before. Here we present new data for the composition of minerals of the mantle xenoliths (clinopyroxene, garnet, phlogopite, K-richterite, and oxides) together with the Sr-Nd isotopes of garnet xenocrysts and whole-rock samples from the Carolina kimberlite. Using these data we provide novel information about a recycling process and the metasomatism of the base of the lithospheric mantle beneath the Amazonian Craton.

2. Geological setting

In Brazil, the majority of kimberlitic fields are widespread along an oriented direction of NW-SE (Fig. 1), including well-known occurrences of alkaline rocks (e.g., kamafugite, lamproite, lamprophyre, ultramafic lamprophyre, and carbonatite) in Rondônia, Mato Grosso and Minas Gerais states (Gonzaga and Tompkins, 1991; Gibson et al., 1995, 1997, 2005; Carlson et al., 1996, 2007; Heaman et al., 1998; Brod et al., 2000; Araujo et al., 2001; Sgarbi et al., 2004; Read et al., 2004; Masun and Smith, 2008; Melluso et al., 2008; Hunt et al., 2009; Kaminsky et al., 2010; Guarino et al., 2013; Felgate, 2014; Weska et al., 2020; Carvalho et al., 2022). Considering the chronology of these alkaline rocks, the kimberlites from Rondônia, within the Amazonian Craton, records the oldest Paleozoic-Mesozoic ages (Zolinger, 2005; Masun and Smith, 2008; Hunt et al., 2009; Felgate, 2014). However, the voluminous magmatic episode is essentially Cretaceous and concentrated in the Goiás Alkaline Province (GAP) and the Alto Paranaíba Igneous Province (APIP) (e.g., Gibson et al., 1995; Sgarbi et al., 2004; Guarino et al. 2013; Felgate, 2014).

The kimberlitic intrusions of Rondônia are located in the southwestern border of the Amazonian Craton, distributed in Pimenta Bueno, Colorado D'Oeste, and Ariquemes kimberlitic fields (Cabral Neto et al., 2014). These intrusions are emplaced in the Paleo- Mesoproterozoic (1.82–1.54 Ga) basement rocks from the Rondônia-Juruena Province (Santos et al., 2000, 2008; Pinho et al., 2003; Santos, 2003; Rizzotto et al., 2013 and references therein), and in the Neoproterozoic sedimentary rocks of the Pimenta Bueno Formation (Gaia, 2014).

The Pimenta Bueno Kimberlite Field comprises 54 igneous intrusions distributed in four main clusters: Carolina, Cosmos-Pepper, Arara, and Encanto (Cabral Neto et al., 2017). The diamondiferous Carolina kimberlite, located in the Espigão D'Oeste municipality, intrudes the Serra da Providência Intrusive Suite, which is a rapakivi A-type granite with 1.61–1.53 Ga (Bettencourt et al., 1999; Santos, 2003). The Carolina cluster is represented by the Carolina kimberlite with 1.2 ha diatreme facies, and by the Cometa-1 kimberlite that is a small dike (Hunt et al., 2009; Cabral Neto et al., 2014, 2017). The available geochronological data indicate a Triassic age for the emplacement of the Carolina pipe (232 ± 2.3 Ma Rb-Sr model age on phlogopite; Hunt et al., 2009). Cosmos-1 (226.6 ± 7.2 Ma Rb-Sr methods using phlogopite) and Pepper-13 (237 ± 9 Ma U-Pb perovskite ages) clusters consist, predominantly, of pipes with surficial areas varying between 1 and 12 ha filled with crater- and diatreme facies kimberlite (Masun and Smith, 2008). Felgate (2014) obtained a 2-point Rb-Sr isochron age of 243.9 ± 2.4 Ma for the Cosmos-3 intrusion. Because of their limited dimensions, clusters Arara and Encanto were only superficially studied. Based on garnet, clinopyroxene and whole-rock Sm-Nd isochrons, Zolinger (2005) determined Carboniferous-Permian ages (317 ± 45 and 293 ± 18 Ma) for the Colorado D'Oeste Kimberlitic Field (Concord-2 and Concord-1, respectively). Recently, Felgate (2014) reported a perovskite U-Pb age of 268 ± 9 Ma for the Concord-1 kimberlite. Regarding the Ariquemes Kimberlitic Field in the North-West of the area (Fig. 1), there has no radiometric age been determined for the 12 recognized intrusions. Although mantle xenoliths have been identified in the Carolina kimberlite intrusion (Weska et al., 2020), among others, they have not been the subject of a petrological or geochemical study.

3. Methods and analytical techniques

The 13 mantle xenoliths of this study were carefully selected from drill cores of the Carolina kimberlite intrusion. They are small, varying from 3 to 5 cm across. The xenoliths were firstly studied with an optical microscope, but as most of them are strongly altered, the petrographic description was difficult (see Fig. 2A, C). Therefore, these samples were mostly characterized based on Scanning Electron Microscope (SEM) analyzes together with backscattering (BSE) images. This initial characterization was done with a Quanta 450 - FEI SEM equipped with energy dispersive spectroscopy (EDS), backscattering (BSE) and secondary electron (SE) detectors, at the Laboratório de Geocronologia e Geoquímica Isotópica, Universidade de Brasília, Brazil.

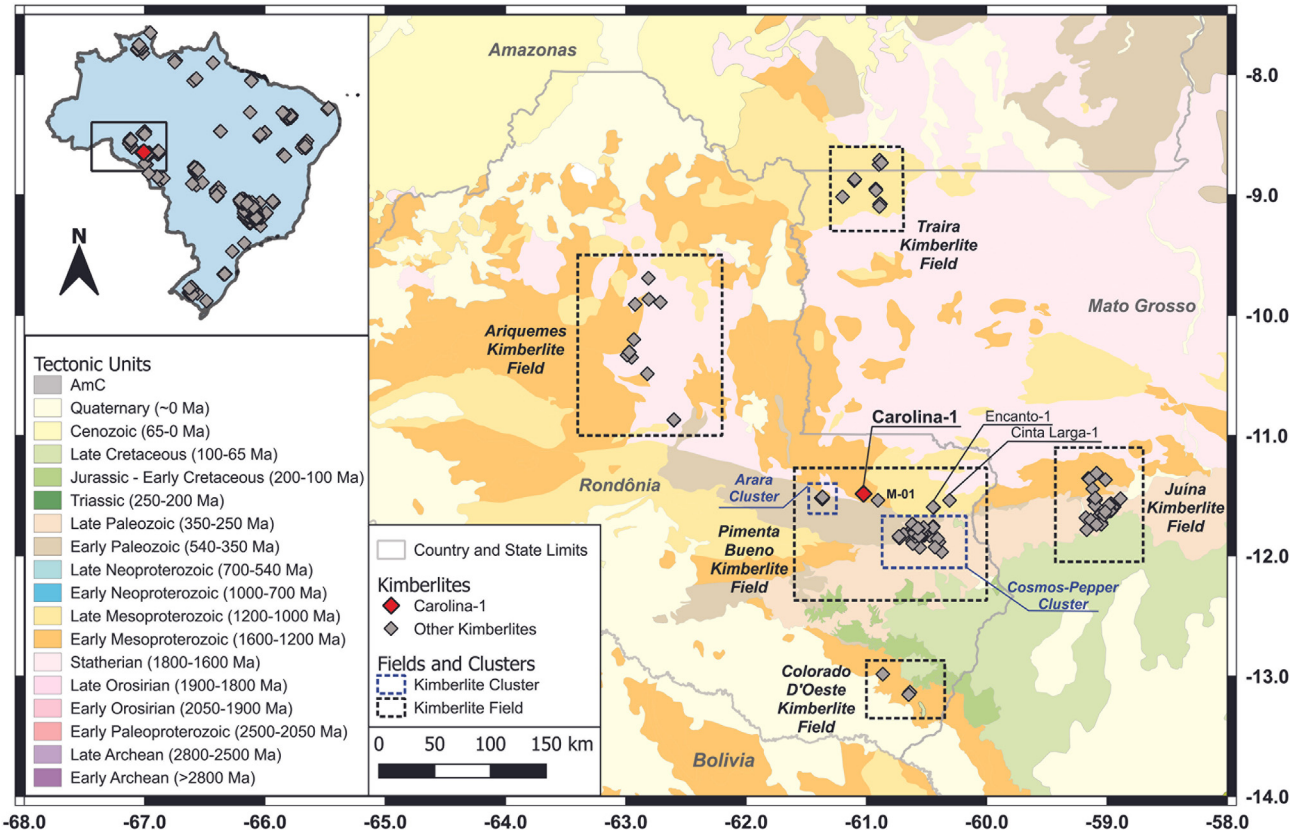

Fig. 1. Kimberlitic intrusions of the southwestern border of Amazonian Craton, distributed in Pimenta Bueno, Colorado D'Oeste, and Ariquemes kimberlite fields in the Rondônia State, and Traíra and Juína kimberlite fields in Mato Grosso State.

Due to alteration of some samples, it was not possible to analyze trace element compositions of clinopyroxenes from all samples, neither the K-richterite minerals. Analyzes of mineral major elements using the Electron Probe Micro Analyzer (EPMA) were possible because of the help of the SE and BSE images, but LA-ICP-MS analyzes were hindered by the difficulty to find the minerals with the optical microscope of the laser ablation system. Therefore, in this study we present trace element analyzes only from clinopyroxenes of samples RW-23B, CA-04, CA-05 and CA-07 (Supplementary Data, Table S1), and none trace element analyzes of K-richterites.

3.1. Mineral chemistry

Mineral major element concentrations were measured using an EPMA in two laboratories. Samples RW-298, RW23B, RW27A, RW27B, RW28A, RW28B, were analyzed with a JEOL JXA-8530F at the Institute of Mineralogy, University of Münster, Germany. The other samples were analyzed using a JEOL JXA-8900 at the Laboratório de Microssonda Eletrônica, Instituto de Geociências, Universidade de Brasília, Brazil. The analyzes with both microprobes were done with an acceleration voltage of 15 kV, a beam current of 10 nA and a beam diameter of 1 μm in the spot mode. In each laboratory, analyzes of silicate minerals were run according to the in-house method. In Münster, standards used for quantitative measurements were hypersthene (Si), rutile (Ti), disthene (Al), fayalite (Fe), rhodonite (Mn), forsterite (San Carlos olivine) (Mg), diopside (Ca), jadeite (Na), sanidine (K), chromite (Cr) and nickel oxide (Ni). In Brasília, measurements were calibrated with the following standards: andradite (Ca and Fe), albite (Na), forsterite (Mg), microcline (K, Al and Si), pyrophanite (Ti and Mn), chromium oxide (Cr), and nickel oxide (Ni).

Trace element concentrations were obtained using laser ablation inductively coupled plasma mass spectrometry (LA-ICP-MS) at the Institute of Mineralogy, University of Münster, Germany. For samples RW-298, RW23B, RW27A, RW27B, RW28A, RW28B, a Thermo Scientific Element 2 ICP-MS was used, and the other samples were analyzed using a Thermo Scientific Element XR ICP-MS. Both ICP-MS were coupled to a 193 nm ArF excimer laser (Teledyne PhotonMachines Analyte G2) ablation system. Minerals were analyzed with a laser repetition rate of 5 Hz using a fluence of about 4 J/cm^2. Plasma gas was Ar, and the transport gas was He. The NIST SRM 612 reference glass was used to tune the ICP-MS for maximum sensitivity, stability, and low oxide production rates ($^{232}Th^{16}O/^{232}Th < 0.1\%$). Ablation time was 40 s and the gas blank was measured for 30 s before ablation. The washout time was 20 s. The laser spot size was varied from 60 to 85 μm depending on the size of the crystal. Results were reduced using the GLITTER software (RW-298, RW23B, RW27A, RW27B, RW28A, RW28B; Griffin et al., 2008) and the IOLITE software (other samples; Paton et al., 2011). The selected reference materials (silicate glasses BIR-1G and BHVO-2G) were used to monitor accuracy of the obtained data (see Supplementary Data, Table S2).

3.2. $^{87}Sr/^{86}Sr$ and $^{147}Sm/^{143}Nd$ isotopes

The unspiked $^{87}Sr/^{86}Sr$ isotope ratios and $^{147}Sm/^{143}Nd$ isotope systematics were determined for 29 garnet concentrates, as well as for 6 whole-rock kimberlite samples. Garnets were carefully handpicked under a binocular microscope. Eleven of the garnet crystals are classified as eclogitic (G3), twelve are Ti-metasomatized (G11), and six garnets are lherzolitic (G9) (Table 1). They were mechanically disaggregated from the kimberlite and then only crystals without inclusions and/or any

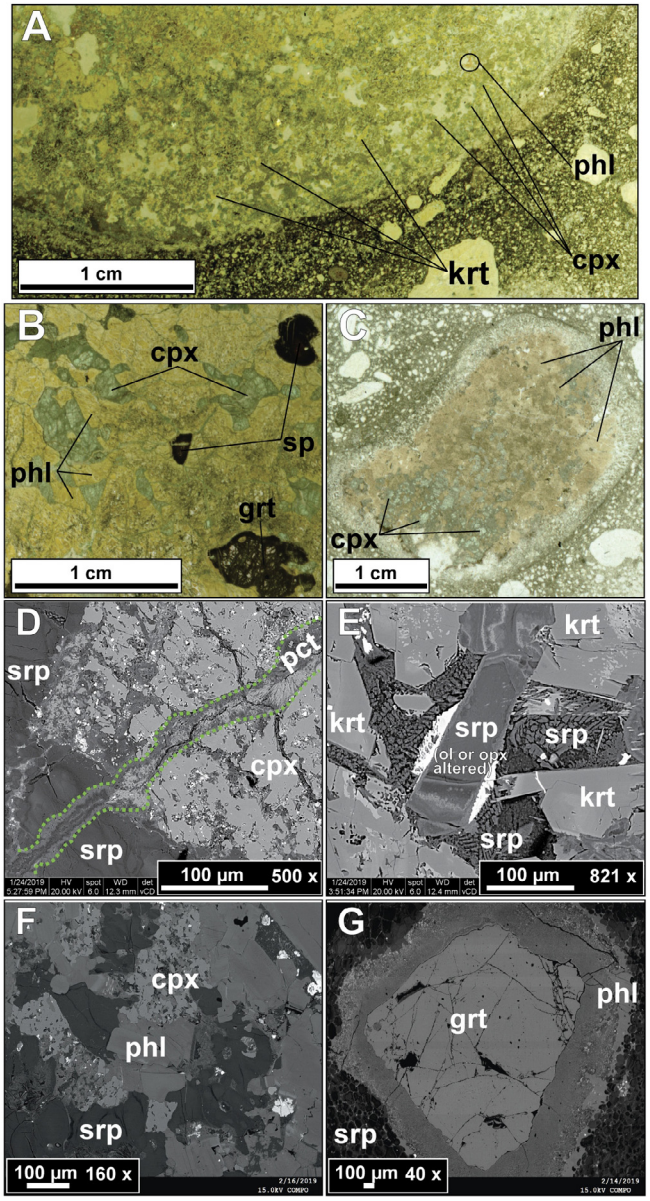

Fig. 2. Scanned images of thin sections from the Carolina kimberlite mantle xenoliths: (A) sample RW-28A, (B) sample RW-23B, and (C) sample CA-05, showing the usual alteration of the samples and the predominance of hydrated minerals (K-richterite in A, and phlogopite in B and C) and clinopyroxenes. (D) Backscatter electron image showing an altered clinopyroxene with veins filled by pectolite (sample RW-23B); (E) euhedral crystals of K-richterite next to serpentine (sample RW-28A); (F) anhedral and lightly altered clinopyroxene next to euhedral phlogopites and serpentine (sample RW327-b); and (G) kelyphitic rims around garnet consisting mainly of phlogopite (sample RW- 298D). For the abbreviations: phl = phlogopite; cpx = clinopyroxene; grt = garnet; Krt = K-richterite; sp = spinel; srp = serpentine; pct = pectolite.

sign of weathering were carefully handpicked under a binocular microscope in order to avoid altered material. The mineral powders were produced manually using an agate mortar and pestle. Individual aliquots of samples were used for Sr (0.1 g; without addition of spike) and Sm and Nd (0.1 g for Sm and 0.5 g for Nd with addition of mixed ^{149}Sm-^{150}Nd spike) isotope analysis. Sample digestion for both analyzes followed the procedure described by Gioia and Pimentel (2000). Sr was separated using Eichrom SR-B100-S (100–150 µm) resin. Sm-Nd were separated in Teflon columns in two steps where the first column procedure used cationic resin AG-50 W-X8 (200–400 mesh) to separate rare earth elements (REE), followed by Sm-Nd separation using anionic Eichrom LN Resin (100–150 µm). Sr and Sm-Nd samples were loaded onto double Re filament assembly and the measurements were carried out by Thermal Ionization Mass Spectrometry (TIMS) through a Thermo-Finnigan Triton mass spectrometer at the Laboratório de Geocronologia e Geoquímica Isotópica, Universidade de Brasília, Brazil. The data were corrected for mass fractionation by normalizing to ^{88}Sr/^{86}Sr value of 8.3752 and ^{146}Nd/^{144}Nd of 0.7219. The analyzes of NIST-SRM NBS-987 and BHVO-2 standards gave ^{87}Sr/^{86}Sr = 0.710255 ± 0.000002 (n = 2, 2σ) and ^{143}Nd/^{144}Nd = 0. 512969 ± 0.000006 (n = 2, 2σ), respectively. These values are compatibles with the reference values of 0.710248 ± 0.00011 (Thirlwall, 1991) and 0.512957 ± 0.000006 (Raczek et al., 2003). Blank values for Nd and Sm are lower than 200 pg.

4. Results

4.1. Petrography

Most of the samples are phlogopite- and clinopyroxene-rich mantle xenoliths (Fig. 2B, C), despite samples RW-28A and RW-28B that have amphibole as the K-rich dominant phase (Fig. 2A), and samples CA-02 and CA-03 that have garnet as the dominant modal phase. Some samples contain a few serpentine pseudomorphs that may indicate the previous presence of olivine and/or orthopyroxene (Fig. 2D, E, F, G). However, since they are few in samples, here we focus on the main modal mineralogy of these rocks. Sample RW-23B is characterized by veins rich in pectolite (Fig. 2D) and have a prominent reaction border when in contact with the kimberlite (Fig. 2C), which may indicate an interaction with the host kimberlite. The other samples do not show such interaction with the host rock. In general, the studied samples have a massive structure. Micas (phlogopite) are large (>50 µm) and euhedral to subhedral crystals (Fig. 2F). Amphiboles (K-richterite) do not show any orientation, are euhedral and have sizes ranging from 30 to 150 µm (Fig. 2E). Clinopyroxenes vary from 20 to >200 µm. Small crystals may be subhedral to euhedral and sometimes are oriented probably following a former metasomatic vein. Larger crystals may contain spinel inclusions (Fig. 2D, F), and are commonly affected by a secondary process, such as those that formed the pectolite veins (Fig. 2D) and/or those that may have caused the clinopyroxene dissolution (Fig. 2F). Garnets are usually subhedral to anhedral with sizes of 20 to 250 µm. Sample RW-298 contains larger garnets (1 to 2.5 cm) at the border of the xenolith that show kelyphitic rims forming a layer of mica around it. As secondary and accessory phases, apatite, titanite, carbonates, barite, and other non-identified sulfides were detected with the SEM (Table 2).

Due to the predominance of micas and clinopyroxenes, most of the samples can be classified as mica clinopyroxenites (Table 2). Two mica clinopyroxenites also contain garnet, spinel, ilmenite and rutile (Table 2) and two samples contain K-rich amphibole + clinopyroxene + spinel (Fig. 2A, E) and were hence classified as K-richterite clinopyroxenites (Table 2). Considering that two samples have garnet as their dominant mineral phase, they were classified as mica-clinopyroxene garnetites. One sample consists of serpentine, garnet and phlogopite (Fig. 2G), and it is classified as garnet-mica peridotite (as serpentine reflects the previous presence of olivine and/or orthopyroxene).

4.2. Mineral chemistry

All mineral compositions are given in the Supplementary Material (Supplementary data, Tables S1, S3-S9). Major and trace

Table 1
Sr-Nd isotopic ratios of pyrope garnets and whole-rock kimberlites from Carolina.

Sample	Rock/Mineral	Sm (ppm)	Nd (ppm)	$^{147}Sm/^{144}Nd$	$^{143}Nd/^{144}Nd$	2σ	ε_{Nd}	$^{87}Sr/^{86}Sr$	2σ
G3-A1	Garnet	0.479	0.622	0.4653	0.512871	0.000008	4.6	0.70572	0.00004
G3-A2	Garnet	-	-	-	-	-	-	0.70576	0.00001
G3-A3	Garnet	0.526	0.359	0.8856	0.513478	0.000028	16.4	0.70513	0.00001
G3-A4*	**Garnet**	**0.541**	**0.649**	**0.5042**	**0.513001**	**0.000008**	**7.1**	**0.70723**	**0.00003**
G3-A5*	**Garnet**	**0.736**	**0.551**	**0.8069**	**0.513568**	**0.000019**	**18.2**	**-**	**-**
G3-A6*	**Garnet**	**0.713**	**0.532**	**0.8112**	**0.513614**	**0.000016**	**19.0**	**0.7076**	**0.00001**
G3-B2*	**Garnet**	**0.187**	**0.255**	**0.4426**	**0.512903**	**0.000012**	**5.2**	**-**	**0.00001**
G3-B3	Garnet	1.003	1004	0.6041	0.513117	0.000016	9.4	-	0.00002
G3-B4	Garnet	0.531	0.522	0.6152	0.513280	0.000017	12.5	0.70963	0.00002
G3-B5	Garnet	1.172	0.951	0.7455	0.513620	0.00001	19.2	-	-
G3-B6*	**Garnet**	**0.953**	**0.664**	**0.8669**	**0.513707**	**0.000018**	**20.9**	**-**	**-**
G11-R01	Garnet	0.793	0.932	0.5141	0.513186	0.000013	10.7	-	-
G11-R02	Garnet	0.488	0.606	0.4868	0.513564	0.000013	18.1	-	-
G11-R03	Garnet	0.609	0.674	0.5459	0.513493	0.000013	16.7	-	-
G11-R04	Garnet	0.491	0.638	0.466	0.513313	0.000037	13.2	-	-
G11-R05	Garnet	0.463	0.539	0.519	0.513347	0.000012	13.8	0.70606	0.00002
G11-R06	Garnet	0.547	0.682	0.4847	0.513295	0.000015	12.8	-	-
G11-RX1	Garnet	0.747	0.9	0.5013	0.513247	0.000020	11.9	0.70713	0.00002
G11-RX2	Garnet	0.781	0.925	0.5106	0.513298	0.000015	12.9	0.70634	0.00001
G11-RX3	Garnet	0.672	1.14	0.3562	0.513042	0.000020	7.9	0.70817	0.00002
G11-RX4	Garnet	0.547	0.951	0.3478	0.512958	0.000012	6.2	0.71098	0.00002
G11-RX5	Garnet	0.593	0.693	0.5168	0.513414	0.000023	15.1	0.71015	0.00001
G11-RX6	Garnet	1.304	1.64	0.4807	0.513114	0.000022	9.3	-	-
G9-1	Garnet	0.543	0.423	0.7767	0.513660	0.000004	19.9	0.70405	0.00001
G9-2	Garnet	0.681	0.815	0.5046	0.513232	0.000005	11.6	-	-
G9-3	Garnet	0.576	0.621	0.561	0.513179	0.000005	10.6	0.70459	0.00002
G9-4	Garnet	0.642	0.669	0.5802	0.513495	0.000017	16.7	-	-
G9-5	Garnet	0.578	0.591	0.5916	0.513554	0.000017	17.9	0.70616	0.00002
G9-6	Garnet	1.097	1.264	0.525	0.513254	0.000004	12.0	-	-
RW32X	Kimberlite WR	22.73	140.37	0.0979	0.512580	0.000008	-2.3	0.706335	0.000002
RW33	Kimberlite WR	20.55	139.34	0.0892	0.512553	0.000007	-1.7	0.705749	0.000001
RW06	Kimberlite WR	17.20	104.52	0.0994	0.512573	0.000009	-1.3	0.705689	0.000002
RW04	Kimberlite WR	25.06	164.75	0.092	0.512562	0.000014	-1.5	0.705840	0.000002
RW05	Kimberlite WR	17.26	116.20	0.0898	0.512548	0.000020	-1.8	0.705498	0.000002
RW07	Kimberlite WR	45.64	113.34	0.2434	0.512583	0.000009	-1.1	0.706871	0.000002
NBS-987	-	-	-	-	-	-	-	0.71027	0.000002
NBS-987	-	-	-	-	-	-	-	0.71028	0.000002

The uncertainties are 2**σ**. G3 = eclogitic, G9 = lherzolitic, and G11 = Ti-metasomatized garnets. WR = whole-rock.
*Samples selected to construct the Sm-Nd isochron age.

Table 2
Mineralogical assemblage and classification of the 13 studied ultramafic mantle xenoliths from Carolina kimberlite.

Sample	Main phases (and identified accessory phases)	Classification
RW-298	Phl + Grt	Garnet-Mica-bearing peridotite*
RW-327B	Phl + Cpx + Sp + (ap)	Mica clinopyroxenite
RW-23B	Phl + Grt +Cpx + Sp + (ap + sulf)	Garnet-Mica clinopyroxenite
RW-27A	Phl + Grt + Cpx + Ilm + Rt + (cc + ttn)	Garnet-Mica clinopyroxenite (Eclogite?)
RW-27B	Phl + Grt + Cpx + (ap + cc + ttn + bar)	Garnet-Mica clinopyroxenite (Eclogite?)
RW-28A	Cpx + Krt + Sp + (ap + ttn + bar)	K-richterite bearing clinopyroxenite
RW-28B	Phl + Cpx + Krt + Sp + (ap)	K-richterite bearing clinopyroxenite
CA01	Phl + Cpx + (cc)	Mica clinopyroxenite
CA02	Phl + Grt + Cpx + (cc)	Mica-Cpx garnetite
CA03	Phl + Grt + Cpx + Ilm + Sp + Rt + (cc)	Mica-Cpx garnetite
CA04	Phl + Cpx	Mica clinopyroxenite
CA05	Phl + Cpx + (ap + cc)	Mica clinopyroxenite
CA07	Phl + Cpx	Mica clinopyroxenite

* = sample formed by serpentine, garnet and phlogopite.
Phl = Phlogopite; Cpx = Clinopyroxene; Grt = Garnet; Krt = K-richterite; Sp = Spinel; Ilm = Ilmenite; Rt = Rutile; cc = carbonate (calcite); ap = apatite; sulf = sulfides non-identified; ttn = titanite; bar = barite.

element data (as displayed in Figures and Tables) are only from mineral cores to avoid any altered parts of the mineral rims.

4.2.1. Major elements

4.2.1.1. Clinopyroxene. Clinopyroxenes (except CA-02 and CA-03) have Mg# [100 × Mg/(Mg + Fe_t) molar] ranging from 85 to 95 (Supplementary data, Table S3). They are diopside-rich with Ca# [100 × Ca/(Ca + Mg) molar] from 44 to 54, with low TiO_2 (<1.15 wt.%), and with a wide variation of Na_2O (0.40–2.35 wt.%), Cr_2O_3 (0.23–3.57 wt.%) and Al_2O_3 (0.02–9.13 wt.%) concentrations (Fig. 3; Supplementary Data, Table S3). Clinopyroxenes from samples CA-02 and CA-03 have different compositions, mainly defined by their low Mg# (79–81) and high Al_2O_3 contents (7.20–14.55 wt.%). They are Al-rich diopsides with high Ca# (49–63), low Cr_2O_3 (<0.15 wt.%), and variable TiO_2 (0.26–1.75 wt.%) and Na_2O (0.20–2.64 wt.%) contents.

Clinopyroxenes with Na_2O > 2 wt.%, when compared to Cr_2O_3 and CaO contents, have similar compositions to clinopyroxenes

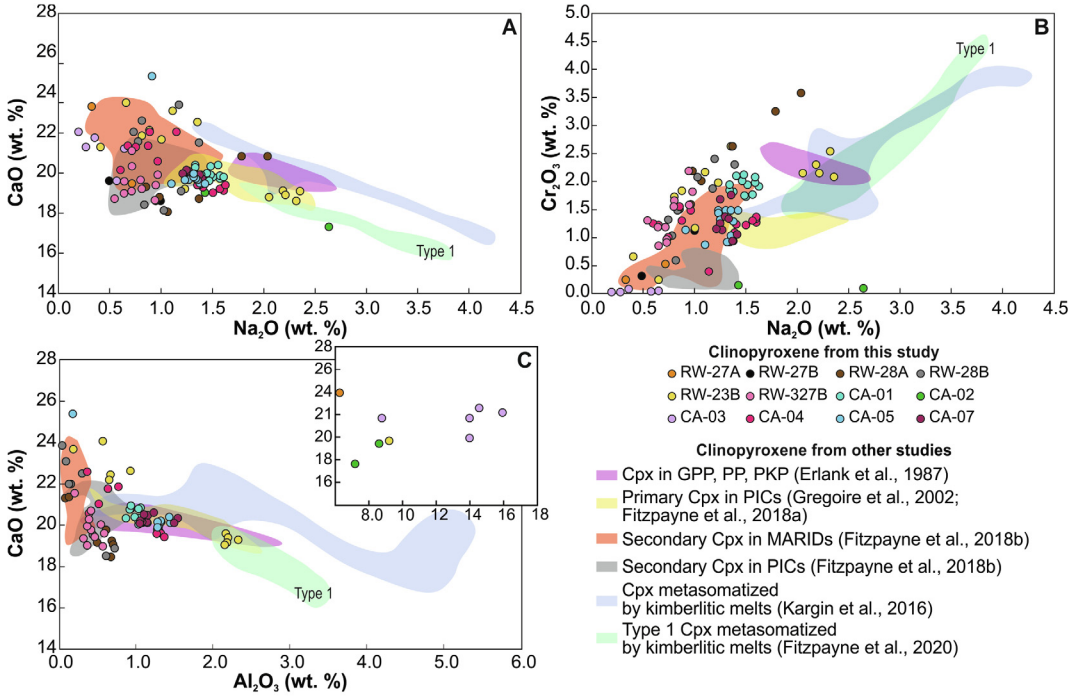

Fig. 3. Major element compositions of clinopyroxenes from Carolina mantle xenoliths plotted with clinopyroxenes formed by the interaction between mantle xenoliths and kimberlitic melts at mantle dephts (Kargin et al., 2016; type 1 cpx from Fitzpayne et al., 2020), primary clinopyroxenes found in GPP, PP and PKP (Erlank et al., 1987), in MARIDs and PICs (Gregoire et al., 2002; Fitzpayne et al., 2018a; type 2 cpx from Fitzpayne et al., 2020), and secondary clinopyroxenes present in MARIDs and PICs formed by reaction with kimberlitic melts (Fitzpayne et al., 2018b).

formed by proto-kimberlitic melt (silicate-carbonate melt) and/or by kimberlitic metasomatism (Fig. 3A and B) (Kargin et al., 2016; type 1 cpx from Fitzpayne et al., 2020), which reflects such increase in Na_2O. Moreover, samples with low Na_2O and low Cr_2O_3 plot close to the field of those primary clinopyroxenes from PIC (phlogopite–ilmenite–clinopyroxene) xenoliths (Fig. 3B) (Gregoire et al., 2002; Fitzpayne et al., 2018a; type 2 cpx from Fitzpayne et al., 2020), as well as with secondary clinopyroxenes present in veins found in MARIDs and PICs caused mainly by kimberlitic infiltration (Fitzpayne et al., 2018b). In terms of the Ca/Al ratio, clinopyroxenes display a large variation (3–416), with sample RW-28B showing the highest Ca/Al ratio of 1571. A few clinopyroxene grains from samples RW-27A, RW-23B, and all clinopyroxenes from samples CA-02 and CA-03 have Ca/Al ratios lower than 5, with CA-02 and CA-03 having the lowest ratios (Ca/Al = 2–3). All the other clinopyroxenes from RW-327B, RW-28A, RW27-B, CA-01, CA-02, CA-04, CA-05 and CA-07 have high Ca/Al ratios (10–416).

4.2.1.2. Mica. Micas are phlogopite with variable concentrations of MgO (13.51–28.63 wt.%) and FeO (3.14–12.65 wt.%), resulting in Mg# ranging from 67 to 93. Micas from samples CA-03 (Mg# = 67–76), RW-27A (Mg# = 82–85) and RW-27B (Mg# = 82–91) show the highest variation in Mg# compared to the other samples. They are also enriched in FeO_t, close to the annite endmember (Supplementary Data, Fig. S1). Apart from these three samples, the other micas from the Carolina kimberlite mantle xenoliths have Mg# with constant values between 87 and 93 (Supplementary data, Table S4). Considering the other element compositions, micas display variable concentrations in Al_2O_3 (8.69–19.13 wt.%), TiO_2 (0.46–7.24 wt.%), Cr_2O_3 (<2.32 wt.%) and K_2O (7.94–11.13 wt.%). Micas with the highest Al_2O_3, TiO_2 and FeO_t, together with the lowest Cr_2O_3 and Mg# values (Supplementary data, Table S4) are classified as the annite-rich member and belong to sample CA-03.

The discrimination diagrams comparing Al_2O_3 with TiO_2 and FeO_t contents (Fig. 4A, B), and Mg# with TiO_2 contents (Fig. 4C), display the range of compositions observed in micas of this study. Most of the samples with low FeO_t (<5.0 wt.%) and low TiO_2 (<2.0 wt.%) overlap with primary phlogopite found in GPP, PP, PKP (Erlank et al., 1987) and MARIDs and PICs from the Kaapvaal Craton, South Africa (Gregoire et al., 2002; Fitzpayne et al., 2018a), as well as with phlogopite metasomatized by proto-kimberlitic melts in mantle xenoliths from the Grib Kimberlite, Russia (phlogopite type 2, Kargin et al., 2019). Samples with higher TiO_2 and Al_2O_3, coupled with low Mg#, continue to follow the phlogopite trend formed by metasomatism caused by proto-kimberlitic melts (type 2 phlogopites in Kargin et al., 2019). High TiO_2 and Al_2O_3 phlogopite of this study is also similar in composition to micro and macrocrysts of phlogopite from the Bultfontein kimberlite (Giuliani et al., 2016), groundmass phlogopite from the Grib kimberlite (Kargin et al., 2019) and from typical orangeites of the Bushveld Complex, Kaapvaal Craton in South Africa (Tappe et al., 2021a,b). Such enrichment in TiO_2 and FeO_t is also typical of phlogopite phenocrysts from the Mediterranean lamproites (Serbia, Spain and Turkey; Fritschle et al., 2013), and of the ultramafic lamprophyres from the Aillik Bay, at the southern edge of the North Atlantic Craton (Tappe et al., 2006).

4.2.1.3. Garnet. Garnets are present in six mantle xenoliths from the Carolina kimberlite (see Table 2). In sample RW-27A it was possible to analyze only remnants of garnets. Garnets are pyrope-almandine rich, with the solid solution ranging from 33 to 74 mol% pyrope and from 14 to 41 mol% almandine. The most almandine-rich garnets are samples RW-27A, RW-27B, CA-02 and CA-03, which are also the most depleted in Cr_2O_3 (<0.14 wt.%), with Mg# between 44 and 78 (Supplementary Data, Table S5). Samples RW-298 and RW-23B are pyrope-rich and have Cr_2O_3 concentrations ranging from 3.47 to 5.42 wt.%, and Mg# between 74 and

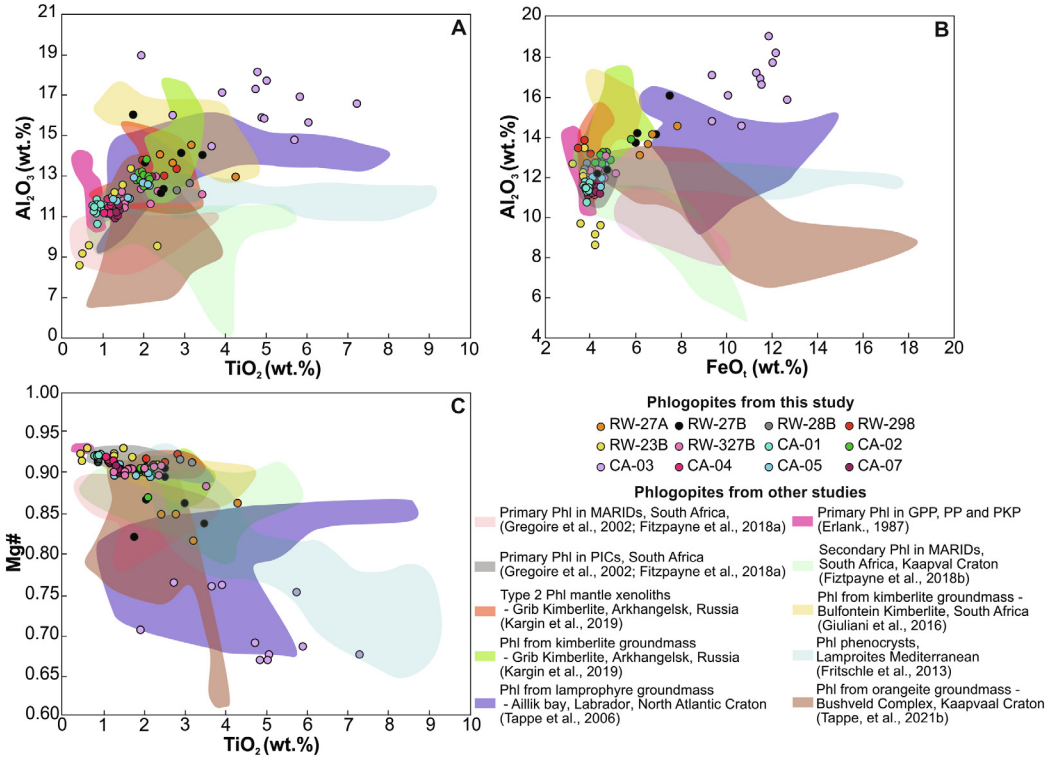

Fig. 4. Phlogopite major element compositions from Carolina kimberlite mantle xenoliths. Our data are compared to other primary phlogopite from the GPP, PP and PKP suite (Erlank et al., 1987) and in MARIDs and PICs of kimberlites from the Kaapvaal Craton, South Africa (Gregoire et al., 2002; Fitzpayne et al., 2018a), secondary phlogopite found in veins of MARIDs from the Kaapvaal Craton, South Africa (Fitzpayne et al., 2018b), secondary phlogopite of mantle xenoliths formed by kimberlitic metasomatism (Giuliani et al., 2016; type 2 phlogopites in Kargin et al., 2019), micro and macrocysts from the Bultfontein kimberlite (Giuliani et al., 2016) and from typical orangeites of the Bushveld Complex, Kaapvaal Craton in South Africa (Tappe et al., 2021b), and phlogopite phenocrysts from Mediterranean lamproites (Fritschle et al., 2013), and from the lamprophyres from the Aillik Bay, Labrador, at the southern edge of the North Atlantic Craton (Tappe et al., 2006).

83. They show their distinct compositions from the other garnets comparing MgO versus FeO and MgO versus CaO (Supplementary Data, Fig. S2A, B). Garnets have MnO from 0.21 to 0.46 wt.%, and CaO concentrations varying from 4.42 to 9.60 wt.%. Based on the TiO_2 content, garnets show variations from 0.04 to 0.45 wt.% that is typical of garnets from mantle peridotites (<0.5 wt.%; e.g., Pivin et al., 2009; Schulze, 2003; Kargin et al., 2016), and different from the megacryst garnets with high TiO_2 composition 0.48–1.56 wt.%) from sheared peridotites from the Premier kimberlite, Kaapvaal Craton (Tappe et al., 2021a).

In terms of the classification scheme proposed by Grütter et al. (2004), pyrope-rich garnets from RW-23B and RW-298 mantle xenoliths plot in the harzburgitic (G10) field (Supplementary data, Fig. S2C). On the other hand, the almandine-rich samples (RW-27A, RW-27B, CA-02 and CA-03) are classified as G4 and G3 fields, which belong to pyroxenitic and eclogitic garnets, respectively (Supplementary Data, Fig. S2C). It is important to note that considering the mineralogy of almandine-rich samples and the chemical composition of their garnets, they are classified as possible eclogites and garnetites.

4.2.1.4. Amphibole. Amphiboles are present in samples RW-28A and RW-28B. They are classified as potassic (K-) richterite considering their high K_2O (4.58–4.81 wt.%) and Na_2O (4.27–4.85 wt.%) contents (Supplementary data, Table S6). They display CaO concentrations varying from 5.55 to 6.45 wt.%, FeO_t from 1.28 to 2.59 wt.%, TiO_2 from 0.25 to 1.51 wt.%, and low Al_2O_3 concentrations varying from 0.11 to 0.64 wt.%. K-richterite from this study have higher Cr_2O_3 and lower FeO_t abundances compared to K-richterite from MARID rocks from the Kaapvaal Craton, South Africa (Gregoire et al., 2002; Fitzpayne et al., 2018a).

4.2.1.5. Oxides. Oxides in the mantle xenoliths from the Carolina kimberlite are mainly rutile, ilmenite and spinel. Rutile was found in sample RW-27A (one grain) and CA-03, with TiO_2 ranging from 91.18 to 100 wt.% (Supplementary data, Table S7). One crystal of Mg-rich ilmenite is present in sample RW-27A, with TiO_2 = 55.93-wt.%, FeO = 36.67 wt.%, and MgO = 6.16 wt.%. In sample CA-03, the analysis of an unique ilmenite crystal resulted in TiO_2 = 55.06 wt.%, Al_2O_3 = 14.48 wt.%, FeO = 13.32 wt.%, and MgO = 6.94 wt.% concentrations. Spinels display more than one mineral among the spinel series and show intense variations in the solid solutions. The most abundant spinel is Cr-rich in composition (RW-23B, RW-28A, RW-28B, RW-327B) with Cr# ranging from 74 to 99 [where Cr# = 100 × Cr/(Cr + Al)], and with the main solid solutions occurring between Mg-Fe, and Al-Cr. Cr-rich spinels show abundances in FeO_t from 19.05 to 32.66 wt.%, MgO from 4.40 to 13.24 wt.%, TiO_2 from 0.83 to 6.03 wt.%, and Al_2O_3 from 0.23 to 12.11 wt.%. In sample RW-23B, it is also present an Al-rich spinel, with Al_2O_3 concentrations ranging from 41.82 to 47.53 wt.%, Cr_2O_3 from 16.96 to 21.89 wt.%, FeO_t 13.88 to 14.28 wt.%, and MgO from 19.30 to 18.29 wt.%. Magnetite (FeO_t = 82.85 wt.%) and Fe-rich spinel (Al_2O_3 = 59.53 wt.%, FeO_t = 21.86 wt.%, MgO = 16.80 wt.%) are present in sample CA-03.

4.2.2. Trace elements

4.2.2.1. Clinopyroxene. Here we show trace element compositions of clinopyroxenes from samples RW-23B, CA-04, CA-05 and CA-07 (Supplementary data, Table S1). Most of these clinopyroxenes show that the high field strength elements (HFSE), such as Nb, Ta, Zr, Hf, are enriched compared to the primitive mantle (PM; Sun and McDonough, 1989). However, Nb and Ta contents in some minerals show slightly lower concentrations compared to PM, and

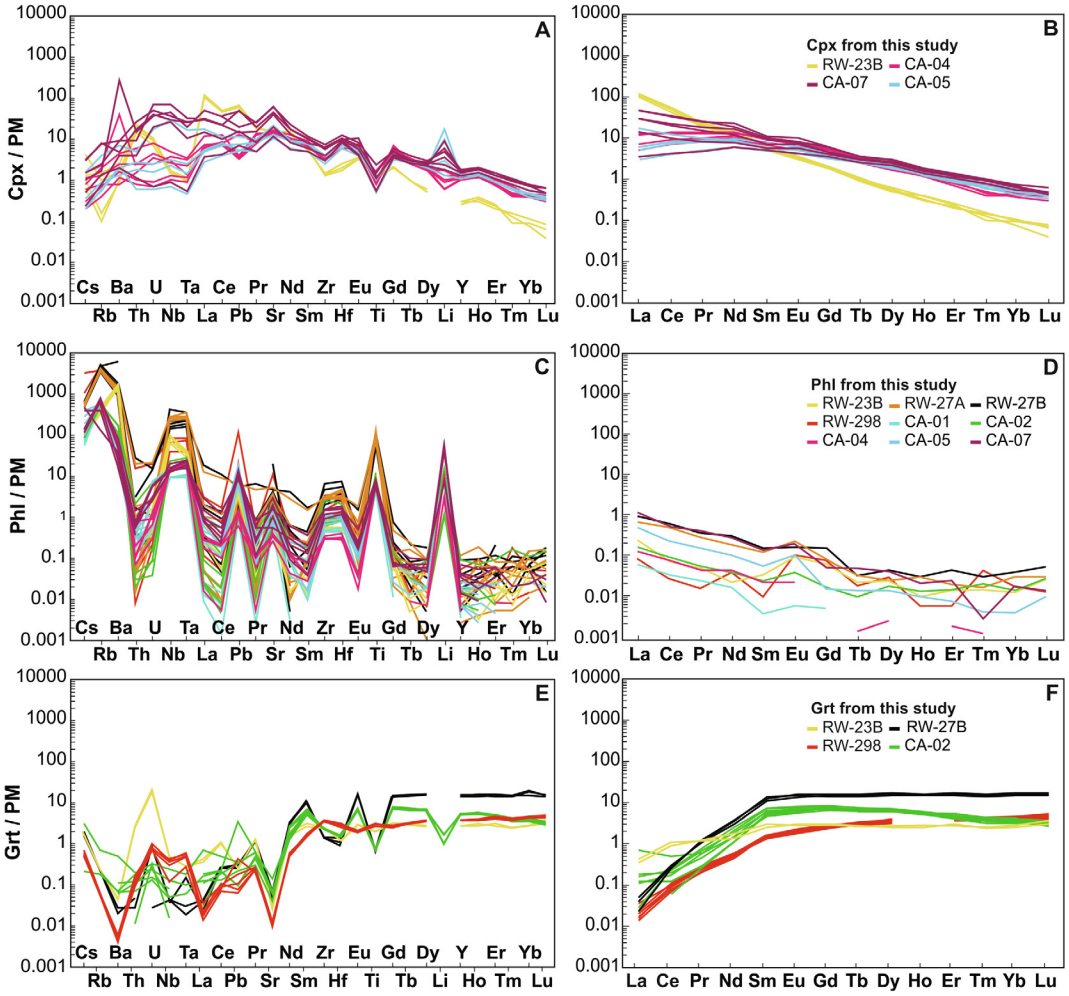

Fig. 5. Trace and REE element patterns of clinopyroxenes (A-B), phlogopites (C-D), and garnets (E-F) from the Carolina kimberlite mantle xenoliths. The trace element and the REE data were normalized to the primitive mantle (Sun and McDonough, 1989). The phlogopite REE diagram (B) shows the average concentration of phlogopite core analyzes, whereas the others show individual measurements for each mineral.

all minerals contain negative anomalies in Ti (Fig. 5A). The HFSE ratios display variations, such as Zr/Hf from 13 to 26, Nb/Ta from 18 to 44, and the Ti/Eu ratio varies from 742 to 2840. In terms of large-ion lithophile elements (LILE), samples show positive anomalies in Sr and Ba, and have variable Rb contents (Fig. 5A). Clinopyroxenes show light REE (LREE) concentrations compared to the heavy (H-) and middle (M-) REE (La_N/Yb_N = 5–62; Ce_N/Sm_N = 1–3) (Fig. 5B), especially the sample RW-23B that has the highest LREE/HREE ratio (La_N/Yb_N = 962–1446; Ce_N/Sm_N = 7–8).

4.2.2.2. Phlogopite. Phlogopite trace element compositions are quite similar (Fig. 5C), with positive anomalies in Pb, Sr and Li, and in the HFSE (Nb, Ta, Zr, Hf and Ti) (Fig. 5C). Phlogopite is enriched in Cs, Rb and Ba, and most samples are depleted in U and Th compared to the primitive mantle. Despite the similar patterns observed at the PM-normalized diagram (Fig. 5C), the studied micas show significant variation in element contents, such as in Rb (150–786), Ba (15–1824) and Nb (9–98) (all data normalized to PM). In general, the REE contents in the studied phlogopite (only the average contents are shown for each sample) have low abundances and define a slightly inclined depleted patterns compared to the primitive mantle (Fig. 5D), mainly for the HREE (La_N/Yb_N = 0.3–114.8; Ce_N/Yb_N = 0.1–84.8; all samples with REE < 1 × PM).

4.2.2.3. Garnet. Garnets from sample RW-27A are remnants of crystals that could be well observed in the microprobe but could not be found and analyzed at the LA-ICP-MS. Despite this sample, trace elements from garnets of this study present variable patterns in several elements, with negative anomalies of the LILEs Ba and Sr (Fig. 5E). Samples RW-27B (possible eclogite) and CA-02 (garnetite) also display enrichment in Eu and depletion in Ti (Fig. 5E). The Li concentration was detected only in garnets from sample CA-02, showing a negative anomaly compared to the neighbour elements. The REE PM-normalized diagram shows typical patterns for garnets with LREE<HREE (Ce_N/Yb_N = 0.01–0.36, and Sm_N/Er_N = 0.33–1.49) (Fig. 5F).

4.3. $^{87}Sr/^{86}Sr$ and $^{147}Sm/^{143}Nd$ isotopic data

The Sr-Nd isotopic ratios of garnets and whole-rock samples from the Carolina kimberlite are presented in Table 1. Among the 29 analyzed garnets, it was possible to determine 28 Nd and 15 Sr isotope ratios, where 14 samples have their Sr-Nd compositions plotted in the Fig. 6A. Garnets show high to very high $^{143}Nd/^{144}Nd$ isotope ratios (0.51287–0.51371) and εNd (+4.55 to +20.85; n = 21 measurements higher than 10) coupled with enriched $^{87}Sr/^{86}Sr$ isotope ratios (0.70405–0.71098) (Fig. 6A). In general, these samples define a scattered and near-horizontal pattern defined by the

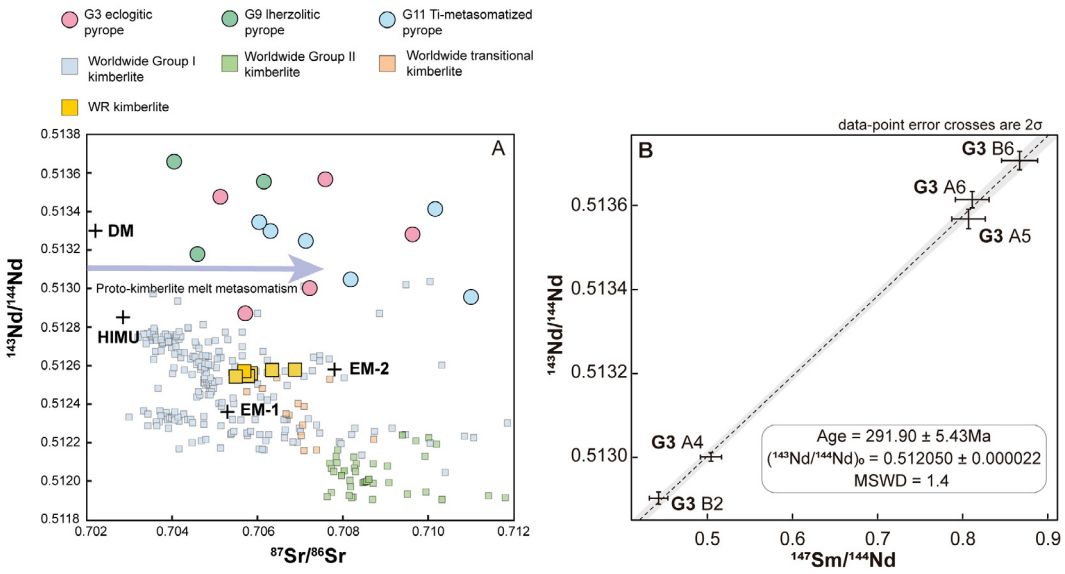

Fig. 6. The diagram A shows Sr-Nd isotopic composition of garnet xenocrysts from Carolina mantle xenoliths (G3 eclogitic, G9 lherzolitic and G11 Ti-metasomatized), as well as of whole-rock host kimberlite. For comparison, are plotted the depleted mantle (DM), HIMU, enriched mantle 1 (EM1) and enriched mantle 2 (EM2) mantle end-members (Hart et al., 1992); worldwide kimberlites from Group 1 and Group 2 (Orangeites) and Transitional kimberlites (Nowell et al., 2004; Becker and Le Roex, 2006; Becker et al., 2007; Coe et al., 2008; Tappe et al., 2017, 2020, 2021b, and references therein). The diagram B shows Sm–Nd isochron age for eclogitic garnet xenocrysts from Carolina kimberlite. The uncertainties are 2σ. Based on five mineral concentrates, it was possible to determine the radiometric age of 291.9 ± 5.4 Ma, with $^{143}Nd/^{144}Nd$ initial ratio of 0.51205 ± 0.00002 and MSWD = 1.4.

Sr-Nd isotope compositions, where lherzolite garnets contain the lower Sr (0.70405–0.70616) ratios at a given high-Nd ratios (0.51318–0.51317) compared to Ti-metasomatized and eclogite samples (Fig. 6A). Whole-rock kimberlite isotope ratios ($^{87}Sr/^{86}Sr$ = 0.70550–0.70687; $^{143}Nd/^{144}Nd$ = 0.51255–0.51258) plot between the enriched mantle 1 (EM-1) and enriched mantle 2 (EM-2) (Hart et al., 1992), with εNd varying from −1.07 to −2.34 (Fig. 6A and Table 1).

Eclogitic garnets were employed to construct an Sm-Nd isochron, producing an age of 291.9 ± 5.4 Ma, with initial $^{143}Nd/^{144}Nd$ of 0.51205 ± 0.00002 (2σ) (MSWD = 1.4) (Fig. 6B and Table 1). This Paleozoic age is slightly older than Mesozoic age obtained for the emplacement of the host kimberlite (232 ± 2.3 Ma; Hunt et al., 2009), as well as with other kimberlite intrusions of Pimenta Bueno (Cosmos-1 = 227 Ma; Cosmos-3 = 244 Ma; Pepper-13 = 23 7 Ma; Masun and Smith, 2008; Felgate, 2014).

4.4. P-T estimates

Pressure and temperature estimates were calculated using the PTEXL geothermobarometry spreadsheet (created by Thomas Köhler in the 1990s and modified and updated by Thomas Stachel in 2019) using the mineral core compositions (Supplementary data, Tables S3, S4, S5). Few geothermobarometers from this spreadsheet could be applied in the studied mantle xenoliths due to their lack of preserved olivine and orthopyroxene and due to their intense metasomatism. Garnet-mica clinopyroxenites (RW-27A, RW-27B and RW-23B) attended the criteria required to have temperatures estimated by geothermometers based on the exchange of Fe and Mg between clinopyroxene and garnet (Ellis and Green, 1979; Powell, 1985; Krogh, 1988; Krogh, 2000). Additionally, the single clinopyroxene thermometer by Nimis and Taylor (2000) could be applied for most of the samples (garnet-mica clinopyroxenites, mica-pyroxenites and K-richterite bearing clinopyroxenites). For pressure estimates, the best geobarometer suitable for most of the samples was the single clinopyroxene barometer (Nimis and Taylor, 2000). Garnetites (CA-02 and CA-03) do not have reliable temperature and pressure estimates as their clinopyroxenes are small and restrict to metasomatic pockets. Thus, mantle xenoliths from the Carolina kimberlite were stable in a range of temperature from 855 to 1102 °C, coupled with pressures from 3.6 (~119 km) to 7.0 GPa (~231 km), with most samples stable between 5.2 and 5.7 GPa (170–190 km).

The calculated pressures for samples RW-28A (5.6 GPa) and RW-28B (5.2 GPa), both of which contain K-richterite, agree well with reported pressure of K-richterite (Konzett et al., 1997), which based on experiments determined that the paragenesis K-richterite + clinopyroxene + phlogopite is stable in a range of 4 to 7 GPa, at 1136 °C.

5. Discussion

5.1. Phlogopite and K-richterite rich mantle rocks in the SCLM below the Amazonian Craton

Phlogopite-rich mantle xenoliths are pieces of cratonic mantle commonly found in kimberlites and orangeites from the Kaapvaal Craton, South Africa (e.g., Dawson and Smith, 1977; Gregoire et al., 2002, 2003; Fitzpayne et al., 2018a,b). The most common K-rich mantle xenoliths from the cratonic lithosphere are classified as PIC (Phlogopite-Ilmenite-Clinopyroxene), GPP (Garnet-Phlogopite Peridotite), PKP (Phlogopite-K-richterite-Peridotite), PP (Phlogopite Peridotite) and MARID (Mica–Amphibole–Rutile–Ilmenite–Diopside). The origin of such K-rich ultramafic rocks is still debated, with some authors suggesting that MARID and PIC, for instance, are deep-seated segregations from highly alkaline melts genetically linked to kimberlite magmas (Gregoire et al., 2002); or that these mica-rich rocks are products of K-rich melt metasomatism that had reacted with the mantle lithologies (e.g., Dawson and Smith, 1977; Erlank et al., 1987; Sweeney et al., 1993; Gregoire et al., 2002; Fitzpayne et al., 2018a).

Here we report these types of intensely metasomatized rocks for the first time in Brazil, as mantle xenoliths hosted by kimberlites. The suite of mantle xenoliths brought to the surface by the Carolina kimberlite is composed mainly of phlogopite-rich clinopy-

roxenites. They were derived from 3.6 (~119 km) to 7.0 GPa (~231 km), in which most samples represent a snapshot of the lithosphere-asthenosphere boundary (LAB = 175 km beneath Carolina; Priestley et al., 2018) beneath the Amazonian Craton. Some of them are garnet-bearing, and among them, two samples have K-richterite as the main K-rich mineral phase instead of phlogopite. Since these samples are the first of their kind from the Amazonian cratonic lithosphere, including the K-richterite pyroxenites, it is important to properly classify them to constrain the chemical evolution of this cratonic root.

The classification of the Carolina kimberlite mantle xenoliths can be, in part, constrained by petrographic observations. Despite the intense weathering, we can discard the chance of having MARID and PIC in the studied samples, since these rocks should always contain the paragenesis of Mica–Amphibole–Rutile–Ilmenite–Diopside and Phlogopite-Ilmenite-Clinopyroxene, respectively (e.g., Gregoire et al., 2002). Moreover, MARIDs are also discarded based on the mineral chemical composition when the studied K-richterite and phlogopite are compared to those present in MARIDs from the Bultfontein, Kimberley, and Barkly West areas, Kaapvaal Craton (Erlank et al., 1987; Gregoire et al., 2002; Fitzpayne et al., 2018a) (Figs. 4 and 7A). On the other hand, except phlogopite from garnetites and eclogites that represent slab relicts (CA-03, CA-02, RW-27A and RW-27B, Table 2), K-richterite and phlogopite of this study have similar contents of FeO_t, Cr_2O_3, Al_2O_3 and Mg# compared to primary minerals present in mantle xenoliths classified as PIC, PP, PKP, and GPP (Figs. 4, 7) (Erlank et al., 1987; Gregoire et al., 2002; Fitzpayne et al., 2018a). Since our rocks do not contain ilmenite (apart of RW-27A and CA-03, which are slab relicts) and therefore are not PIC, they have a great chance to be part of a GPP-PP-PKP suite of samples. Moreover, clinopyroxenes of the studied samples have CaO and Al_2O_3 concentrations similar to those found in GPP-PP-PKPs (Fig. 3 C) and are, in general, alike to secondary clinopyroxenes found in veins from MARIDs and PICs from the Kaapvaal Craton (Fig. 3A, B), which formed due to reactions with kimberlitic melts at mantle depths (Fitzpayne et al., 2018a).

Overall, we propose that petrographic and chemically, phlogopite- and K-richterite- clinopyroxenites of the Carolina kimberlite represent a GPP-PP-PKP suite of samples in the deep portion of the cratonic lithosphere beneath the Amazonian Craton. Furthermore, the abundance of K-rich minerals in the studied mantle xenoliths, as well as the chemical similarities of the studied phlogopite and clinopyroxenes with minerals not only from GPP-PP-PKP, but also from PICs, may reflect that an intense metasomatism occurred in the deep lithosphere (most samples were in equilibrium at 170–190 km), probably in the LAB beneath the Amazonian Craton. It has been proposed that PICs and the GPP-PP-PKP suite of rocks have their origin related to metasomatic reactions of lithospheric peridotites with kimberlite melts at mantle depths (Erlank et al., 1987; Fitzpayne et al., 2018a). Therefore, we argue that K-rich metasomatism must have occurred in the lithosphere close to the LAB beneath the Amazonian Craton to form mica-rich pyroxenites.

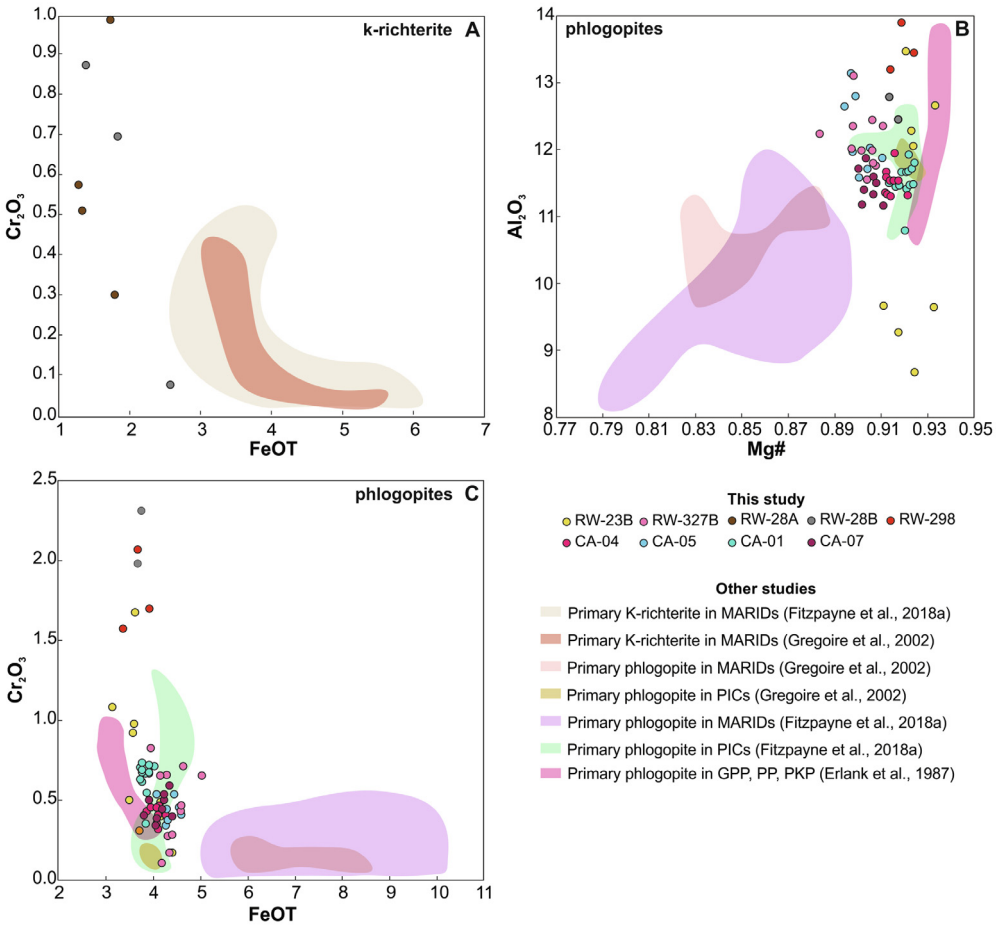

Fig. 7. Variation diagrams of K-richterites and phlogopite compositions from Carolina kimberlite mantle xenoliths. (A) K-richterites are compared to primary K-richterites of MARIDs from Kaapvaal Craton (Gregoire et al., 2002; Fitzpayne et al., 2018a); (B) and (C) Phlogopites from mantle xenoliths of this study are compared to primary phlogopites of MARIDs and PICs from Kaapvaal Craton (Gregoire et al., 2002; Fitzpayne et al., 2018a).

5.2. Effects of proto-kimberlite melt metasomatism on the base of the cratonic lithosphere beneath the Amazonian Craton recorded by clinopyroxene and phlogopite from K-richterite- and phlogopite-pyroxenites

It is widely known that the presence of mica and amphibole in the mineral assemblage of mantle xenoliths indicates modal metasomatism (e.g., O'Reilly and Griffin, 2013). However, the question about the origin of these specific mantle rocks with large amounts of K-rich minerals in their mineral assemblage (e.g., PIC, GPP, PP and PKP) suggests that the lithospheric mantle may have experienced metasomatism caused by melts or fluids enriched in potassium (e.g., Erlank et al., 1987; Sweeney et al., 1993; Fitzpayne et al., 2018a,b), or such rocks are products of K-rich magmas crystallization (e.g., Dawson and Smith, 1977; Jones et al., 1982; Waters, 1987; Gregoire et al., 2002).

Variations of major element compositions of clinopyroxenes from the Carolina kimberlite mantle xenoliths (Fig. 3) exhibit strong similarities with secondary clinopyroxenes from GPP, PP and PKP (Erlank et al., 1987), with secondary clinopyroxenes present in MARIDs and PICs that were formed by reactions with kimberlitic melt at mantle depths (Fitzpayne et al., 2018b), as well as with clinopyroxenes from peridotites that experienced kimberlitic metasomatism in the SCLM (Kargin et al., 2016; type 1 cpx from Fitzpayne et al., 2020). Evidence of possible kimberlitic melt metasomatism affecting clinopyroxenes from the studied mantle xenoliths may be observed even by enrichment in Na_2O and Cr_2O_3, which agrees with the compositions of clinopyroxenes formed after kimberlitic metasomatism (Fig. 3B). Moreover, the abundant occurrence of pectolite in the Carolina kimberlite (Weska et al., 2020) demonstrates such enrichment of Na_2O in the deep lithosphere beneath the Amazonian Craton, which could have affected the mineralogy of the mantle xenoliths.

The high Ca/Al ratios of most clinopyroxenes from phlogopite-rich and K-richterite clinopyroxenites (10–416), coupled with enrichment of LREE relative to HREE (La_N/Yb_N = 5–62; Fig. 5B), could suggest a metasomatism caused by carbonatitic melt in the base of the cratonic lithosphere beneath the Amazonian Craton. However, besides high Ca/Al and La_N/Yb_N ratios, carbonate systems are characterized by high partition coefficient of Zr, Ti, Al and HREE (e.g., Klemme et al., 1995; Blundy and Dalton, 2000; Deng et al., 2017) relative to silicate systems, and therefore, clinopyroxenes that have undergone such kind of carbonatite melt metasomatism would show overall relatively high Zr/Hf and low Ti/Eu ratios. This is not the case for the studied clinopyroxenes that show medium to low ratios of Ti/Eu (742–2840) and relatively low ratios of Zr/Hf (13–26) compared to clinopyroxenes formed from typical carbonatitic metasomatism (e.g., Deng et al., 2017, Zr/Hf = 56–111 and Ti/Eu = 541–969).

In the diagram of La_N/Yb_N versus Ti/Eu ratios (Fig. 8A), firstly suggested by Rudnick et al. (1993) to discriminate carbonatite and silicate melt metasomatism in the mantle, it can be observed that clinopyroxenes from this study present high La_N/Yb_N ratios and higher Ti/Eu ratios compared to those clinopyroxenes formed by metasomatism of carbonatite melts (Coltorti et al., 1999; Deng, et al., 2017) (Fig. 8A). It is also observed in Fig. 8A the similarities of the studied samples with clinopyroxenes from peridotites affected by silicate-carbonate melts similar in composition to kimberlite (Kargin et al., 2016; Fitzpayne et al., 2018b, 2020), and with secondary clinopyroxenes found in veins from MARIDs and PICs that reacted with kimberlitic melts (Fitzpayne et al., 2018b). Moreover, as it is shown in the diagram of Zr/Hf versus Zr (Fig. 8B), the studied clinopyroxenes show lower Zr/Hf ratios compared to samples metasomatized by carbonatitic melts (Deng et al., 2017). On the other hand, they are similar in composition to those formed by kimberlitic or proto-kimberlitic melts metasomatism (Kargin et al., 2016; Fitzpayne et al., 2018b, 2020). Tappe et al. (2017, 2021a and references therein), suggest that CO_2-rich silicate melts (e.g. kimberlites) commonly present in the base of cratonic lithosphere, may have high HFSE concentrations, such as Zr, Hf and Ti. Also, in the LAB, it is accepted that most of the melts present in such region are not only poor carbonated, but silicate-carbonate melts considering the reducing conditions of such deep region (Tappe et al., 2017, 2021a). Therefore, regarding to all these chemical features related to major and trace element compositions, as well as the similarity with clinopyroxenes

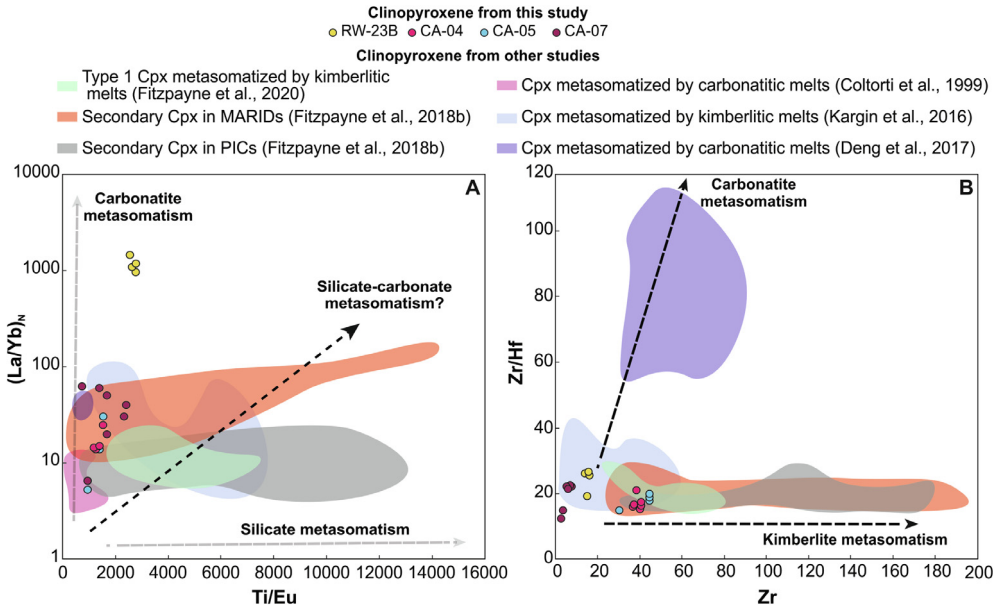

Fig. 8. Plots of La/Yb (PM-normalized) versus Ti/Eu (A), and Zr/Hf versus Zr (B) of studied clinopyroxenes from Carolina kimberlite mantle xenoliths. For comparison, were plotted clinopyroxenes formed by carbonatitic metasomatism (Coltorti et al., 1999; Deng et al., 2017); secondary clinopyroxenes found in MARIDs and PICs formed by kimberlitic metasomatism (Fitzpayne et al., 2018b, 2020), and clinopyroxenes of peridotites that were affected by kimberlitic or proto-kimberlitic metasomatism (Kargin et al., 2016; Fitzpayne et al., 2020).

formed by carbonatitic and kimberlitic melt metasomatism, we propose that the studied clinopyroxenes are products of the metasomatism caused by CO_2-rich silicate melts, similar to proto-kimberlite melts already proposed as a metasomatic agent in other cratonic roots (e.g., Giuliani et al., 2014, 2016; Kargin et al., 2016; Tappe et al., 2021a).

In addition, major element composition of phlogopites from the Carolina kimberlite mantle xenoliths define two well-defined compositional trends related to their TiO_2 concentrations. Phlogopites with TiO_2 higher than 2.0 wt.% are similar to phlogopites of mantle xenoliths formed by kimberlitic metasomatism, as well as with phlogopites from the groundmass of kimberlites, lamproites and lamprophyres (Tappe et al., 2006; Fritschle et al., 2013; Giuliani et al., 2016; Kargin et al., 2019) (Fig. 4A, C). These phlogopites are also enriched in Al_2O_3 (>12.0 wt.%) and FeO_t (5.0–13.0 wt.%) (Fig. 4A, B). In contrast, phlogopites with TiO_2 between 1.0 and 2.0 wt.% coupled with Al_2O_3 lower than 12.0 wt.% are correlated to those usually present in PIC and MARID rocks (Fig. 4A, C). A few samples have even lower TiO_2 (<1.0 wt.%), which is a common concentration found in phlogopites from GPP-PP-PKP suite of rocks (Erlank et al., 1987), in primary phlogopites from mantle xenoliths of kimberlites (e.g., Kargin et al., 2019), as well as phlogopites in equilibrium with the garnet lherzolite mineral assemblage in upper mantle conditions (Carswell, 1973; Kargin et al., 2019). Also, most phlogopites from the Carolina kimberlite mantle xenoliths have low Cr_2O_3 concentrations (<1.0 wt.%; except for samples RW-298 and RW-28B, with Cr_2O_3 from 1.58 to 2.32 wt.%).

The high-Ti phlogopites are usually reported as micas found in the kimberlite groundmass or as high-Ti rims of micas from mantle xenoliths that reacted with kimberlitic melts at mantle depths (e.g., Giuliani et al., 2016; Kargin et al., 2019). To form such K- and Ti-rich minerals it is necessary that the lithospheric mantle lithologies react with a metasomatic agent that has such high alkalinity coupled with Ti affinity. It is well known that the base of cratonic lithosphere is highly affected by different types of metasomatic agents that could be fluids or melts arising from the asthenosphere or even from low degrees of partial melting of the already metasomatized lithosphere (e.g., Foley, 2008; Gervasoni et al., 2017). The metasomatic agents that may affect the cratonic mantle are frequently related to carbonatite and/or K-rich melts/fluids (e.g., Foley, 2008), or hydrous ultramafic silicate-carbonate melts, which are similar in composition to what could be a proto-kimberlitic melt (Gervasoni et al., 2017). Giuliani et al. (2016) proposed that high Ti-Cr phlogopite rims in mantle xenoliths from the Bultfontein kimberlite represent the product of a reaction of "failed" kimberlitic melts that did not reach the surface but instead stalled and metasomatized the lithospheric mantle. Tappe et al. (2018) also suggest that kimberlite magmatism on the surface of cratons represent magma drainage, and not necessary single mantle melting events.

Therefore, considering that part of phlogopites from the Carolina kimberlite mantle xenoliths have high-Ti compositions, we propose that they were formed by early pulses of kimberlite melts that do not reach the surface, but instead progressively interacted with parts of the mantle wall rocks of the base of the lithospheric mantle beneath Amazonian Craton, as suggested by Giuliani et al. (2014, 2016) and Tappe et al. (2016, 2018). Phlogopites from the Carolina kimberlite mantle xenoliths show a wide compositional variation, with some of them showing low-Ti concentrations as typical of primary phlogopites in the mantle (Carswell, 1973; Kargin et al., 2019), or phlogopites present in GPP-PP-PKP suite of rocks (Erlank et al., 1987). However, most of them show considerably increase of Ti content, suggesting that such variation is caused by progressive reaction of Ti- and K-rich melts, possibly related to an ultrapotassic proto-kimberlite melt that interacted to some parts of lithospheric mantle forming the high-Ti phlogopites. As most metasomatized phlogopites have low Cr_2O_3, it is possible that such ultrapotassic proto-kimberlite melts fractionated Cr-rich spinels before reacting with the Carolina mantle xenoliths, reflecting in such low Cr concentration in the metasomatized micas.

5.3. Proto-kimberlite melt percolation and Carolina kimberlite emplacement

The Sr-Nd isotopic ratios of garnet xenocrysts (G3 eclogitic, G9 lherzolitic and G11 Ti-metasomatized) from the Carolina kimberlite suggest selective enrichment of Sr (0.70405–0.71098; most <0.708) at a given high Nd isotopic ratios (0.51287–0.51371; εNd = +4.55 to +20.85) (Fig. 6A). The whole-rock Sr-Nd isotopic ratios of host kimberlite ($^{87}Sr/^{86}Sr$ = 0.70550–0.70687; $^{143}Nd/^{144}Nd$ = 0.51255–0.51258; εNd = −1.07 to −2.34) are strong related to those defined by worldwide Group 1 kimberlites (Nowell et al., 2004; Becker and Le Roex, 2006; Becker et al., 2007; Tappe et al., 2017; Tappe et al., 2020 and references therein) (Fig. 6A). They plot close to the Transitional kimberlite composition (Nowell et al., 2004; Becker et al., 2007), showing no correlation with Group 2 kimberlites (Nowell et al., 2004; Becker and Le Roex, 2006; Coe et al., 2008; Tappe et al., 2021b). Although the $^{87}Sr/^{86}Sr$ ratios of whole-rock Carolina kimberlite do not reach the higher values presented by garnet xenocrysts, the widely scattered compositional distribution of Group 1 kimberlites ($^{87}Sr/^{86}Sr$ up to 0.71963, not shown) or even the compositional trend of Group 2 kimberlites ($^{87}Sr/^{86}Sr$ up to 0.71182; Fig. 6A) justify the metasomatized mantle source beneath the Amazonian Craton (Fig. 6A). Moreover, the initial $^{143}Nd/^{144}Nd$ isotopic ratio ($t_{292\ Ma}$ = 0.51205) of eclogitic garnets attests a strongly enriched (metasomatized) mantle, consistent with diamondiferous regions.

The emplacement age of the Carolina kimberlite was previous determined as Triassic (232 ± 2.3 Ma) based on a Rb-Sr model age on phlogopite (Hunt et al., 2009). Our new Permian Sm-Nd isochron age of 291.9 ± 5.4 Ma was defined through eclogitic garnet macrocrysts. We consider our result more consistent than the previous one due to the isotopic systematic employed, where a Sm-Nd isochron age constructed using 5 points containing a well-defined compositional scattering ($^{147}Sm/^{144}Nd$ = 0.443–0.867 and $^{143}Nd/^{144}Nd$ = 0.51290–0.51371; MSWD = 1.4) offers more reliability than a Rb-Sr model age. It is corroborated by the high incompatibility (and mobility) of Rb and Sr compared to REEs such as Sm and Nd. Hence, Rb-Sr isotopic composition is very sensitive, susceptible to perturbation that promoting the increasing of $^{87}Sr/^{86}Sr$ values while $^{143}Nd/^{144}Nd$ isotopic ratios remaining constant.

The Sr-Nd isotope distribution pattern and a Sm-Nd isochron age recorded by garnet megacrysts, which is ~ 60 Ma older than the previous age determined for the host kimberlite (Hunt et al., 2009), suggest that these garnets were in isotopic equilibrium at the time of the proto-kimberlite melt percolation into the lithosphere-asthenosphere boundary beneath the Amazonian Craton and subsequent Carolina kimberlite eruption. Therefore, this age can be assumed as representatively close to the Carolina kimberlite emplacement. Note that this assumption is supported by the fact that garnet xenocrysts show equilibrium temperatures higher (855–1002 °C) than typical closure temperature for Sm-Nd system in garnet (750–900 °C; Koornneef et al., 2017 and references therein). The closure temperature of garnet in Sm-Nd is dependent on number of variables, such as elemental diffusivity, grain size, cooling rate (or in the case of garnets recording posterior tectonic/metasomatic event such as, here, the duration of the thermal event), and the initial temperature (T_0) from which the rock cools (e.g., Dodson, 1973; Ganguly and Tirone 1999; Van Orman et al., 2002; Shu et al., 2014; Koornneef et al., 2017).

Considering that eclogite garnets from cratonic regions usually have between 5 and 8 mm (Shu et al., 2014), and that the elemental diffusivity is directly related to the grain size, we conclude that the eclogitic garnet xenocrysts of the Carolina kimberlite (<5 mm) used to obtain the Sm-Nd isochron age are highly susceptible to be isotopically replaced by their interaction with the proto-kimberlite melt. Therefore, there is no doubt that our cooling ages are product of proto-kimberlite metasomatism instead the age of oceanic crust metamorphism within the slab recycling.

5.4. Recycling and metasomatic process in the base of the lithospheric mantle beneath the Amazonian Craton

The presence of garnets in mantle xenoliths with eclogitic composition (CA-02, CA-03, RW-27A, RW-27B), as well as the presence of garnetites (CA-02 and CA-03) that are products of metasomatic reactions from subducted-derived melts/fluids (e.g., Smith and Griffin, 2005; Su et al., 2019), defines strong evidence that the lithospheric mantle beneath the Amazonian Craton retained pieces of slabs derived from an ancient subduction zone. Eclogitic garnets are common xenocryst in kimberlites, and eclogites are a typical lithology present in the deep portions of the cratonic lithosphere. Although it was not possible to determine the age of the oceanic crust eclogitization during its recycling into the oceanic trench related with the subduction of the ancestral Farallon plate (Panthalassa Ocean), the cooling age of eclogitic garnet xenocrysts from the Carolina kimberlite (291.9 ± 5.4 Ma), related to the K-rich metasomatic process, indicates that they were metamorphized early than the tectonic context of Proto- and Early-Andean, denominated Gondwana cycle (~330–280 Ma; Oliveros et al., 2020 and references therein).

The western margin of the South American continent has been involved in subduction processes related to the oceanic lithosphere under the Panthalassa Ocean since the Late Paleozoic, when it was still part of the supercontinent Pangea (Boschman and van Hinsbergen, 2016). These ancient plates must have been completely consumed and interacted with the mantle beneath the South American continent. Several studies based on seismic tomography have identified the presence of remnant slabs in the lower mantle, resulting from old subductions (e.g., van der Meer et al., 2010, 2012, 2018; Chen et al., 2019). Numerical modelling results show that different parameters define the geometry of the slab subduction, allowing its direct penetration into the lower mantle or remaining stagnant in the transition zone (Agrusta et al., 2017). Depending on such parameters, the slab can take from tens to hundreds of millions of years to reach the lower mantle. Based on the integration of continent paleogeographical reconstructions (Matthews et al., 2016) and global seismic tomography model (MIT-P08 - Li et al., 2008), it was possible to define that between 287 and 277 Ma, the current position of the Carolina kimberlite was located atop an ancient subducted slab present in the convecting upper mantle to the transition zone, and such slab is probably related with the Farallon Plate (Fig. 9; van der Meer et al., 2012; Boschman and van Hinsbergen, 2016).

In Fig. 9, it is observed that there are high-velocity anomalies in the lower mantle that coincide with the western edge of South America in their paleopositions around 287–277 Ma. The dimension of this anomaly along the entire western margin suggests that

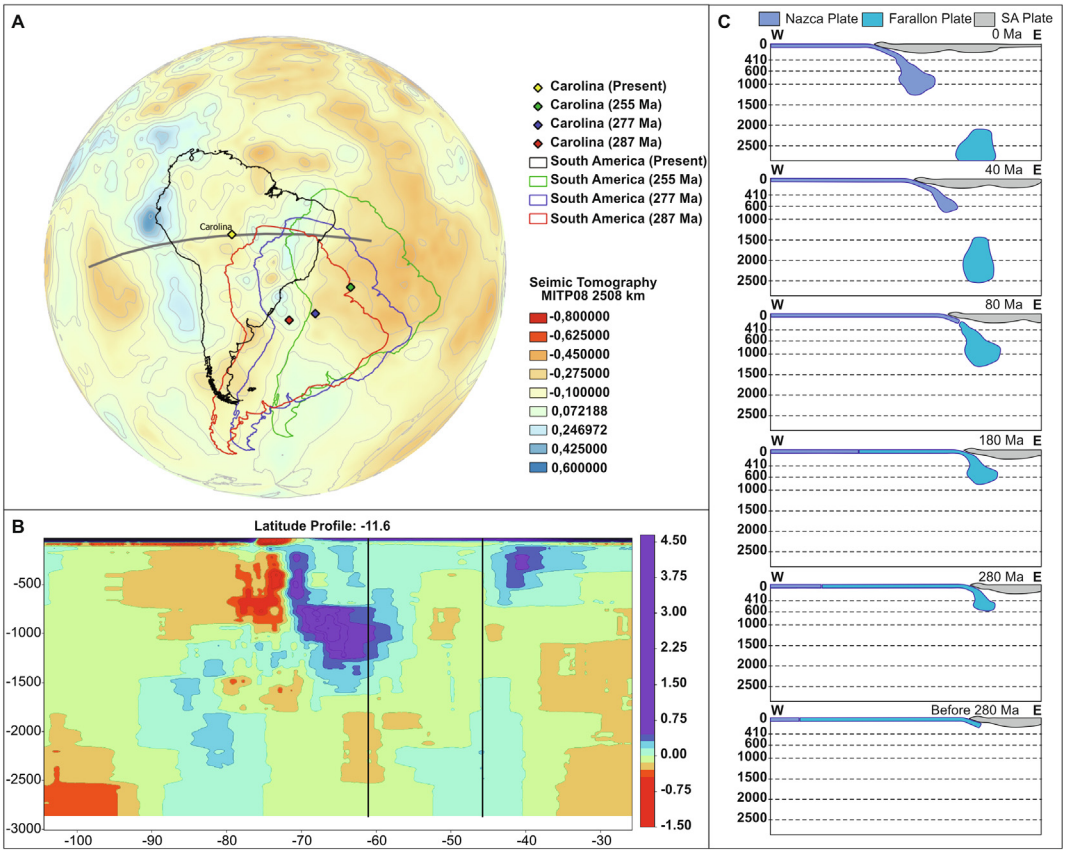

Fig. 9. Comparison between global P-wave seismic tomography anomalies and paleogeographical position of the South America, and interpretation of the evolution of the slab dip in the lower mantle. (A) P-wave global seismic tomography (MIT-P08, Li et al., 2008) at 2508 km, and the positions of South America and the Carolina kimberlite, today (black), at 255 Ma (green), at 277 Ma (277 Ma), and at 287 Ma (red). (B) Vertical tomographic profile (gray line in "a") crossing the latitude of the current position of the Carolina kimberlite. Vertical black lines are the current and at 287 Ma positions of the Carolina kimberlite (from west to east, respectively). (C) Time evolution of slabs subducting in the western limit of South America.

it is related to a remnant slab developed during the Paleozoic. The anomaly related to this deep slab extends from about 1300 km and reaches depths>2800 km (Fig. 9B), with the vertical projection of the Carolina kimberlite position at 287 Ma (black vertical line on the right in Fig. 9B) coinciding with its central portion. These results suggest that a subduction process would have started before 290 Ma (Fig. 9B) and the slab would have stagnated and accumulated in the transition zone (Fig. 9B, 280–180 Ma), having then detached (Fig. 9B; 80 Ma) and descended vertically to the lower mantle (Fig. 9B, 40–0 Ma).

Previous investigations demonstrated that Permian magmatic and metamorphic rocks (299–252 Ma) were produced within a continental arc system, being widely distributed from at least southern North America toward Chilean territory (Restrepo et al., 2011; Ordóñez-Carmona et al., 2006; Vinasco et al., 2006; Mišković et al., 2009; Viscarret et al., 2009; Reitsma, 2012; Spikings et al., 2016; Coloma et al., 2017; Spikings and Paul, 2019). Therefore, we attribute the formation of eclogitic garnet xenocrysts and garnetites and eclogites of Carolina kimberlite to a subduction that was active during the Gondwana (~540–320 Ma), but before the Pangea stabilization (320–280 Ma).

Furthermore, a K-rich melt metasomatism on the base of the lithosphere beneath the Amazonian Craton is recorded by the isotopic data of the garnet xenocrysts from the Carolina kimberlite and the mineral chemistry data of the hosted mantle xenoliths. The Sr-Nd isotopic data of most garnet xenocrysts from the Carolina kimberlite shows that these minerals record the proto-kimberlite melt percolation into the LAB beneath the Amazonian Craton. Major and trace element compositions of clinopyroxenes and phlogopites from the mica and K-richterite clinopyroxenites also suggest that the base of the lithosphere beneath the Amazonian Craton has experienced an intense metasomatism caused mainly by hydrous CO_2-rich silicate melts enriched in potassium. The studied clinopyroxenes have strong chemical similarities to those found in mantle xenoliths that have reacted with kimberlitic or proto-kimberlitic melts. The composition of most studied phlogopites, on the other hand, are akin to those normally present in phlogopite-rich suite of rocks (e.g., GPP, PP, PKP, MARIDs and PICs), which are rocks formed by deep-seated segregations of kimberlite melts (MARID and PIC, Gregoire et al., 2002), or by reactions with kimberlitic melts and peridotites at mantle depths (e.g., GPP, PP, PKP, Erlank et al., 1987). Also, they show similarities with phlogopites from mantle xenoliths metasomatized by kimberlitic melts and from phlogopites found in kimberlite groundmass. These features, together with the presence of K-richterite in two mantle xenoliths, indicate that the base of the lithosphere beneath Amazonian Craton was metasomatized by hydrous silicate melts rich in potassium, similar to kimberlitic melts.

Therefore, we propose that the studied cratonic lithosphere underwent two important processes. First, much earlier than 290 Ma, a subduction zone affected the western margin of South America. With the slab being under progressive metamorphism, the previous altered oceanic crust turned into eclogites and garnetites (recorded by samples RW-27A, RW-27B, CA-03 and CA02, respectively) and the relict of the metamorphozed slab was attached to the base of the Amazonian Craton. Later, the other event observed is the metasomatism caused by hydrous CO_2-rich silicate melt rich in potassium, that reacted with the lithospheric mantle and formed the mica- and K-richterite pyroxenites and chemically affected the other samples. The Sr-Nd isotopic data of xenocrysts garnets from the Carolina kimberlite shows that these minerals record the proto-kimberlite melt percolation into the LAB beneath the Amazonian Craton. We propose that the metasomatic agent was more likely as pulses of failed proto-kimberlitic melts that fully reacted to the base of the lithospheric mantle beneath the Amazonian Craton and did not reach the surface but helped to form the conduits where the Carolina kimberlite percolated. This metasomatism probably occurred in a short time before that the Carolina kimberlite has formed and brought the suite of xenoliths to the surface. Therefore, we argue that the age of Carolina kimberlite eruption and emplacement should be close to the proto-kimberlitic metasomatism (291.9 ± 5.4 Ma), which is ~ 60 Ma older than previous study (Hunt et al., 2009).

We revoke the chance of this proto-kimberlitic melt metasomatism beneath the Amazonian craton being caused by the proper magma of the Carolina kimberlite. Such affirmation relies on textures present of many pyroxenites in which clinopyroxenes and phlogopites do not show disequilibrium textures, suggesting they were already well formed before being captured by the Carolina kimberlite. There are only two samples (RW-23B and RW-298) that show some interactions with the host kimberlite. In sample RW-23B, it was observed thin veins inside the xenoliths with pectolite crystallized, which is a Na-rich mineral that was also found in the Carolina kimberlite groundmass (Weska et al., 2020). In sample RW-298, garnets with kelyphitic rims are on the border of the xenolith in contact to the kimberlite host, and such texture is a strong indication of reaction with kimberlitic melts during its ascent (e.g., Canil and Fedortchouk, 1999; Spetsius and Taylor, 2002; Bussweiler et al., 2016). However, only the core composition of the minerals from these two samples were analyzed and the rims were avoided because of these interactions with the host kimberlitic.

Moreover, the whole-rock Sr-Nd isotopic ratios of host kimberlite ($^{87}Sr/^{86}Sr$ = 0.70550–0.70687; $^{143}Nd/^{144}Nd$ = 0.51255–0.51258; εNd = −1.07 to −2.34) are strong related to those defined for African Group 1 and Transitional kimberlites (e.g., Nowell et al., 2004; Becker and Le Roex, 2006; Becker et al., 2007; Tappe et al., 2017; Tappe et al., 2020, 2021b and references therein), and such kimberlite composition could not crystallizes many clinopyroxenes as those clinopyroxenites formed by the metasomatism in the LAB beneath the Amazonian Craton. The proto-kimberlitic melt that reacted to the lithosphere beneath the Amazonian Craton should be a hydrous and ultrapotassic CO_2-rich silicate melt, similar in composition to Group 2 kimberlite (orangeite) to be able to crystallizes such amount of K-rich minerals.

6. Conclusions

This study presents a suite of mantle xenoliths hosted by the Carolina kimberlite, located in the southwestern border of the Amazonian Craton. The mantle xenoliths are composed by 13 samples classified as mica clinopyroxenites, garnet-mica clinopyroxenites, K-richterite clinopyroxenites, mica-clinopyroxene garnetites and garnet-mica peridotite. We also present the Sr-Nd isotope data of the xenocrystic pyrope garnets and of the whole-rock from the Carolina kimberlite.

Pressures estimates defines a mantle column between 3.6 (~119 km) and 7.0 GPa (~231 km), with most samples between 5.2 and 5.7 GPa (170–190 km), concluding that our samples represent the base of the cratonic lithosphere, close to the lithosphere-asthenosphere boundary beneath the Amazonian Craton.

Considering the petrographic observations and the major element composition of K-richterite and phlogopites present in the clinopyroxenites, our study samples are classified as GPP-PP-PKP suite of rocks, being the first one described in Brazil. Nevertheless, the major and trace element compositions of the clinopyroxenes and phlogopite suggest that the base of the lithospheric mantle beneath the Amazonian Craton has undergone an intense metasomatism caused by failed pulses of ultrapotassic proto-kimberlite melts. This interpretation is corroborated by Sr-Nd isotopes of garnet xenocrysts and whole-rock kimberlite. Sm-Nd data for eclogitic

garnet define a Paleozoic (Permian) isochron (291.9 ± 5.4 Ma). This result reflects a cooling age produced by thermal perturbation related to the metasomatism caused by proto-kimberlite melts on the base of the lithosphere beneath the Amazonian Craton. We propose that the Carolina kimberlite eruption and emplacement occurred short after the metasomatic event, suggesting an older age than previous Mesozoic emplacement age (232 ± 2.3 Ma).

Declaration of Competing Interest

The authors declare that they have no known competing financial interests or personal relationships that could have appeared to influence the work reported in this paper.

Acknowledgments

We would like to thank Prof. N. Botelho for contributing with the microprobe analyzes, and also thanks to Beate Schmitte for her help during the microprobe and LA-ICP-MS analyzes in Münster. Thanks goes to DRI – Litoteca de Porto Velho, Residência de Porto Velho (REPO) – CPRM, who kindly provided drill holes of the Carolina kimberlite samples. Thanks also go to Dr. Daniel Evan Portner for fruitful discussion about tomography results. We would like to give special thanks for the excellent editorial work made by Prof. Dr. Kristoffer Szilas. Our thanks also go to the constructive comments and suggestions given by Prof. Dr. Jingao Liu, Prof. Dr. Michael Grégoire and Prof. Dr. Sebastian Tappe, who significantly improved our discussion. This work was supported by FAPDF (Call 03/2018; Process n° 23568.93.50253.24052018) and Serrapilheira Institute (Serra-1709-18152).

Appendix A. Supplementary data

Supplementary data to this article can be found online at https://doi.org/10.1016/j.gsf.2022.101429.

References

Artemieva, I.M., Thybo, H., Cherepanova, Y., 2019. Isopycnicity of cratonic mantle restricted to kimberlite provinces. Earth Planet. Sci. Lett. 501, 13-19. https://doi.org/ 10.1016/j.epsl.2018.09.034.

Aulbach, S., Griffin, W.L., Pearson, N.J., O'Reilly, S.Y., 2013. Nature and timing of metasomatism in the stratified mantle lithosphere beneath the central Slave craton (Canada). Chem. Geol. 352, 153–169.

Aulbach, S., Pearson, N.J., Reilly, S.Y.O., Doyle, B.J., 2007. Origins of xenolithic eclogites and pyroxenites from the Central Slave Craton. Canada. J. Petrol. 48, 1843–1873. https://doi.org/10.1093/petrology/egm041.

Agrusta, R., Goes, S., van Hunen, J., 2017. Subducting-slab transition-zone interaction: Stagnation, penetration and mode switches. Earth Planet. Sci. Lett. 464, 10–23. https://doi.org/10.1016/j.epsl.2017.02.005.

Araujo, A.L.N., Carlson, R.W., Gaspar, J.C., Bizzi, L.A., 2001. Petrology of kamafugites and kimberlites from the Alto Paranaíba Alkaline Province, Minas Gerais. Brazil. Contrib. Mineral. Petr. 142 (2), 163–177.

Aulbach, S., Stachel, T., 2022. Evidence for oxygen-conserving diamond formation in redox-buffered subducted oceanic crust sampled as eclogite. Nat. Commun. 13, 1924. https://doi.org/10.1038/s41467-022-29567-z.

Becker, M., Le Roex, A.P., 2006. Geochemistry of South African On- and Off- craton, Group I and Group II Kimberlites: Petrogenesis and Source Region Evolution. J. Petrol. 47 (4), 673–703. https://doi.org/10.1093/petrology/egi089.

Becker, M., Le Roex, A.P., Class, C., 2007. Geochemistry and petrogenesis of South African transitional kimberlites located on and off the Kaapvaal Craton. S. A. J. Geol. 110 (4), 631–646. https://doi.org/10.2113/gssajg.110.4.631.

Bussweiler, Y., Stone, R.S., Pearson, D.G., Luth, R.W., Stachel, T., Kjarsgaard, B.A., Menzies, A., 2016. The evolution of calcite-bearing kimberlites by melt-rock reaction: evidence from polymineralic inclusions within clinopyroxene and garnet megacrysts from Lac de Gras kimberlites, Canada. Canada. Contrib, Mineral, Petrol, 171, 65. doi: 10.1007/s00410-016-1275-3.

Bettencourt, J.S., Tosdal, R.M., Leite, W.B., Payolla, B.L., 1999. Mesoproterozoic Rapakivi Granites of the Rondônia Tin Province, Southwestern Border of the Amazon Craton, Brazil: I-reconnaissance U-Pb geochronology and regional implications. Precambrian Res. 95, 41–67.

Blundy, J., Dalton, J., 2000. Experimental comparison of trace element partitioning between clinopyroxene and melt in carbonate and silicate systems, and implications for mantle metasomatism. Contrib. Mineral. Petrol. 139 (3), 356–371.

Boschman, L.M., van Hinsbergen, D.J.J., 2016. On the enigmatic birth of the Pacific Plate within the Panthalassa Ocean. Sci. Adv. 2, (7). https://doi.org/10.1126/sciadv.1600022 e1600022.

Brod, J.A., Gibson, S.A., Thompson, R.N., Junqueira-Brod, T.C., Seer, H.J., de Moraes, L. C., Boaventura, G.R., 2000. The kamafugite-carbonatite association in the Alto Paranaíba Igneous Province (APIP) southeastern Brazil. Revista Brasileira de Geociências 30 (3), 408–412. https://doi.org/10.25249/0375-7536.2000303408412.

Cabral Neto, I., Nannini, F., Silveira, F.V., Cunha, L.M., 2017. Projeto Diamante Brasil, Áreas kimberlíticas e diamantíferas do estado de Rondônia. Série pedras preciosas 11, 1–85.

Cabral Neto, I., Castro, C.C., Silveira, F.V., Cunha, L.M., Weska, R.K., Souza, W.S., 2014. Intrusões kimberlíticas de Rondônia: uma síntese com base no conhecimento atual. In: 6° Simpósio Brasileiro de Geologia do Diamante. Patos de Minas. Volume 1, 97-102.

Canil, D., Fedortchouk, Y., 1999. Garnet dissolution and the emplacement of kimberlites. Earth Planet. Sci. Lett. 167, 227–237. https://doi.org/10.1016/S0012-821X(99)00019-9.

Carlson, R.W., Araújo, A.L.N., Junqueira-Brod, T.C., Gaspar, J.C., Brod, J.A., Petrinovic, I.A., Hollanda, M.H.B.M., Pimentel, M.M., Sichel, S., 2007. Chemical and isotopic relationships between peridotite xenoliths and mafic–ultrapotassic rocks from Southern Brazil. Chem. Geol. 242, 415–434. https://doi.org/10.1016/j.chemgeo.2007.04.009.

Carlson, R.W., Esperanca, S., Svisero, D.P., 1996. Chemical and Os isotopic study of cretaceous potassic rocks from southern Brazil. Contrib. Mineral. Petr. 125 (4), 393–405.

Carswell, D.A., 1973. Primary and secondary phlogopites and clinopyroxenes in garnet lherzolite xenoliths. In: Ahrean, L.H., Duncan, A.R., Erlank, A.J. (Eds.), International Conference on Kimberlites (Extended Abstracts). Pergamon Press, Oxford, Cape Town, South Africa, pp. 417–429.

Carvalho, L.D.V., Jalowitzki, T., Scholz, R., Gonçalves, G.O., Rocha, M.P., Pereira, R.S., Lana, C., Castro, M.P., Queiroga, G., Fuck, R.A., 2022. An exotic Cretaceous kimberlite linked to metasomatized lithospheric mantle beneath the southwestern margin of the São Francisco Craton. Brazil. Geosci. Front. 13,. https://doi.org/10.1016/j.gsf.2021.101281 101281.

Chen, Y.-W., Wu, J., Suppe, J., 2019. Southward propagation of Nazca subduction along the Andes. Nature 565 (7740), 441–447. https://doi.org/10.1038/s41586-018-0860-1.

Coe, N., le Roex, A., Gurney, J., Graham Pearson, D., Nowell, G., 2008. Petrogenesis of the Swartruggens and Star Group II kimberlite dyke swarms, South Africa: constraints from whole rock geochemistry. Contrib. Mineral. Petrol. 156, 627–652. https://doi.org/10.1007/s00410-008-0305-1.

Coloma, F., Valin, X., Oliveros, V., Vásquez, P., Creixell, C., Salazar, E., Ducea, M., 2017. Geochemistry of Permian to Triassic igneous rocks from northern Chile (28°-30°15'S): Implications on the dynamics of the proto-Andean margin. Andean Geol. 44 (2), 147–178.

Coltorti, M., Bonadiman, C., Hinton, R.W., Siena, F., Upton, B.G.J., 1999. Carbonatite Metasomatism of the Oceanic Upper Mantle: Evidence from Clinopyroxenes and Glasses in Ultramafic Xenoliths of Grande Comore, Indian Ocean. J. Petrol. 40, 133–165. https://doi.org/10.1093/petroj/40.1.133.

Dawson, J.B., Smith, J.V., 1977. The MARID (mica–amphibole–rutile–ilmenite–diopside) suite of xenoliths in kimberlite. Geochim. Cosmochim. Acta 41, 309–323.

Deng, L., Liu, Y., Zong, K., Zhu, L., Xu, R., Hu, Z., Gao, S., 2017. Trace element and Sr isotope records of multiepisode carbonatite metasomatism on the eastern margin of the North China Craton. Geochem. Geophys. Geosyst. 18, 220–237. https://doi.org/10.1002/2016GC006618.

Ellis, D.J., Green, D.H., 1979. An experimental study of the effect of Ca upon garnet-clinopyroxene Fe-Mg exchange equilibria. Contrib. Mineral. Petrol. 71, 13–22.

Dodson, M.H., 1973. Closure temperature in cooling geochronological and petrological systems. Contrib. Mineral. Petrol. 40, 259–274.

Erlank, A., Waters, F., Hawkesworth, C., Haggerty, S., Allsopp, H., Rickard, R., Menzies, M., 1987. Evidence for mantle metasomatism in peridotite nodules from the Kimberley pipes. South Africa. In: Menzies, M.A., Hawkesworth, C.J. (Eds.), Mantle Metasomatism. Academic Press, London, pp. 221–311.

Felgate, M.R., 2014. The Petrogenesis of Brazilian kimberlites and kamafugites intruded along the 125° lineament: improved geochemical and geochronological constraints on magmatism in Rondonia and the Alto Paranaiba Igneous Province. The University of Melbourne, p. 275 pp.. Doctoral thesis.

Fitzpayne, A., Giuliani, A., Hergt, J., Woodhead, J.D., Maas, R., 2020. Isotopic analyses of clinopyroxenes demonstrate the effects of kimberlite melt metasomatism upon the lithospheric mantle. Lithos 370–371,. https://doi.org/10.1016/j.lithos.2020.105595 105595.

Fitzpayne, A., Giuliani, A., Hergt, J., Phillips, D., Janney, P., 2018a. New geochemical constraints on the origins of MARID and PIC rocks: Implications for mantle metasomatism and mantle-derived potassic magmatism. Lithos 318–319, 478–493.

Fitzpayne, A., Giuliani, A., Phillips, D., Hergt, J., Woodhead, J.D., Farquhar, J., Fiorentini, M.L., Drysdale, R.N., Wu, N., 2018b. Kimberlite-related metasomatism recorded in MARID and PIC mantle xenoliths. Mineral. Petrol. 112, 71–84.

Fritschle, T., Prelević, D., Foley, S.F., Jacob, D.E., 2013. Petrological characterization of the mantle source of Mediterranean lamproites: Indications from major and

trace elements of phlogopite. Chem. Geol. 353, 267–279. https://doi.org/10.1016/j.chemgeo.2012.09.006.
Foley, S., 1992. Petrological characterization of the source components of potassic magmas: geochemical and experimental constraints. Lithos 28, 187–204.
Foley, S.F., 2008. Rejuvenation and erosion of the cratonic lithosphere. Nature Geosci. 1, 503–510. https://doi.org/10.1038/ngeo261.
Gaia, V.C.S., 2014. A Capa Carbonática do Sudoeste do Cráton Amazônico, Estado de Rondônia: nova Ocorrência e Extensão dos Eventos Pós-Glaciação Marinoana (635 Ma). Universidade Federal do Pará, Dissertação de Mestrado, p. 75.
Ganguly, J., Tirone, M., 1999. Diffusion closure temperature and age of a mineral with arbitrary extent of diffusion: theoretical formulation and applications. Earth Planet. Sci. Lett. 170, 131–140.
Gervasoni, F., Klemme, S., Rohrbach, A., Grützner, T., Berndt, J., 2017. Experimental constraints on mantle metasomatism caused by silicate and carbonate melts. Lithos 282–283, 173–186. https://doi.org/10.1016/j.lithos.2017.03.004.
Gibson, S.A., Thompson, R.N., Leonardos, O.H., Dickin, A.P., Mitchell, J.G., 1995. The Late Cretaceous impact of the Trindade mantle plume: evidence from large-volume, mafic, postassic magmatism in SE Brazil. J. Petrol. 36, 189–229.
Gibson, S.A., Thompson, R.N., Weska, R.K., Dickin, A.P., Leonardos, O.H., 1997. Late Cretaceous rift-related upwelling and melting of the Trindade starting mantle plume head beneath western Brazil. Contrib. Mineral. Petrol. 126, 303–314.
Gibson, S.A., Thompson, R.N., Day, J.A., Humphris, S.E., Dickin, A.P., 2005. Melt generation processes associated with the Tristan mantle plume: Constraints on the origin of EM-1. Earth Planet. Sci. Lett. 237 (3–4), 744–767.
Gioia, S.M.C.L., Pimentel, M.M., 2000. The Sm-Nd isotopic method in the geochronology laboratory of the University of Brasília. Anais da Academia Brasileira de Ciências 72, 219–245. https://doi.org/10.1590/S0001-37652000000200009.
Giuliani, A., Phillips, D., Kamenetsky, V.S., Goemann, K., 2016. Constraints on kimberlite ascent mechanisms revealed by phlogopite compositions in kimberlites and mantle xenoliths. Lithos 240–243, 189–201. https://doi.org/10.1016/j.lithos.2015.11.013.
Giuliani, A., Phillips, D., Kamenetsky, V.S., Kendrick, M.A., Wyatt, B.A., Goemann, K., Hutchinson, G., 2014. Petrogenesis of mantle polymict breccias: insights into mantle processes coeval with kimberlite magmatism. J. Petrol. 55, 831–858.
Gonzaga, G.M.,Tompkins, L.A. 1991. Geologia do Diamante. In: Cap. IV de Principais Depósitos Minerais do Brasil., Vol. IV Parte A - Gemas e Rochas Ornamentais. Coord. Geral: Carlos Schobbenhaus, Emanuel de Teixeira Queiroz e Carlos Eduardo da Silva Coelho, DNPM/CPRM, Brasília/DF. p. 56, 60, 83, 86, 88.
Gregoire, M., Bell, D.R., Le Roex, A.P., 2002. Trace element geochemistry of phlogopite-rich mafic mantle xenoliths: their classification and their relationship to phlogopite-bearing peridotites and kimberlites revisited. Contrib. Mineral. Petrol. 603–625. https://doi.org/10.1007/s00410-001-0315-8.
Gregoire, M., Bell, D.R., Le Roex, A.P., 2003. Garnet lherzolites from the Kaapvaal Craton (South Africa): Trace element evidence for a metasomatic history. J. Petrol. 44, 629–657.
Griffin, W., Powell, W., Pearson, N.J., O'Reilly, S., 2008. GLITTER: data reduction software for laser ablation ICP-MS. Short Course Ser. 40, 308–311.
Grütter, H.S., Gurney, J.J., Menzies, A.H., Winter, F., 2004. An updated classification scheme for mantle-derived garnet, for use by diamond explorers. Lithos 77, 841–857. https://doi.org/10.1016/j.lithos.2004.04.012.
Guarino, V., Wu, F.-Y., Lustrino, M., Melluso, L., Brotzu, P., Gomes, C. De B., Ruberti, E., Tassinari, C.C.G., Svisero, D.P., 2013. U-Pb ages, Sr–Nd- isotope geochemistry, and petrogenesis of kimberlites, kamafugites and phlogopite-picrites of the Alto Paranaíba Igneous Province, Brazil. Chem. Geol. 353, 65-82. doi:10.1016/j.chemgeo.2012.06.016
Hart, S.R., Hauri, E.H., Oschmann, L.A., Whitehead, J.A., 1992. Mantle plumes and entrainment: Isotopic evidence. Science 256, 517–520. https://doi.org/10.1126/science.256.5056.517.
Heaman, L., Teixeira, N.A., Gobbo, L., Gaspar J.C., 1998. U-Pb zircon ages for kimberlites from the Juína and Paranatinga provinces, Brazil. International Kimberlite Conference: Extended Abstracts, 7(1), 322-324. https://doi.org/10.29173/ikc2723.
Herzberg, C., 2004. Geodynamic information in peridotite petrology. J. Petrol. 45, 2507–2530.
Hunt, L., Stachel, T., Morton, R., Grutter, H., Creaser, R.A., 2009. The Carolina kimberlite, Brazil - Insights into an unconventional diamond deposit. Lithos 112, 843–851.
Ionov, D.A., Doucet, L.S., Xu, Y., Golovin, A.V., Oleinikov, O.B., 2018. Reworking of Archean mantle in the NE Siberian craton by carbonatite and silicate melt metasomatism: Evidence from a carbonate-bearing, dunite-to-websterite xenolith suite from the Obnazhennaya kimberlite. Geochim. Cosmochim. Acta 224, 132–153. https://doi.org/10.1016/j.gca.2017.12.028.
Jones, R.A., Smith, J.V., Dawson, J.B., 1982. Mantle metasomatism in 14 veined peridotites from Bultfontein mine, South Africa. J. Geol. 90, 435–453.
Kaminsky, F.V., Sablukov, S.M., Belousova, E.A., Andreazza, P., Tremblay, M., Griffin, W.L., 2010. Kimberlitic sources of super-deep diamonds in the Juina area, Mato Grosso State. Brazil. Lithos 114 (1), 16–29.
Kargin, A.V., Sazonova, L.V., Nosova, A.A., Lebedeva, N.M., Kostitsyn, Y.A., Kovalchuk, E.V., Tretyachenko, V.V., Tikhomirova, Y.S., 2019. Phlogopite in mantle xenoliths and kimberlite from the Grib pipe, Arkhangelsk province, Russia: Evidence for multi-stage mantle metasomatism and origin of phlogopite in kimberlite. Geosci. Front. 10 (5), 1941–1959. https://doi.org/10.1016/j.gsf.2018.12.006.
Kargin, A.V., Sazonova, L.V., Nosova, A.A., Tretyachenko, V.V., 2016. Composition of garnet and clinopyroxene in peridotite xenoliths from the Grib kimberlite pipe, Arkhangelsk diamond province, Russia : Evidence for mantle metasomatism associated with kimberlite melts Grib pipe. Lithos 262, 442–455. https://doi.org/10.1016/j.lithos.2016.07.015.
Klemme, S., van der Laan, S.R., Foley, S.F., Günther, D., 1995. Experimentally determined trace and minor element partitioning between clinopyroxene and carbonatite melt under upper mantle conditions. Earth Planet. Sci. Lett. 133 (3), 439–448.
Konzett, J., Armstrong, R.A., Günther, D., 2000. Modal metasomatism in the Kaapvaal craton lithosphere: constraints on timing and genesis from U-Pb zircon dating of metasomatized peridotites and MARID-type xenoliths. Contrib. Mineral. Petrol. 139, 704–719.
Konzett, J., Sweeney, R.J., Thompson, A.B., Ulmer, P., 1997. Potassium Amphibole Stability in the Upper Mantle: an Experimental Study in a Peralkaline KNCMASH System to 8.5 GPa. J Petrol. 38, 537–568.
Koornneef, J.M., Gress, M.U., Chinn, I.L., Jelsma, H.A., Harris, J.W., Davies, G.R., 2017. Archaean and Proterozoic diamond growth from contrasting styles of large-scale magmatism. Nature Commun. 8, 648. https://doi.org/10.1038/s41467-017-00564-x.
Krogh Ravna, E., 2000. The garnet–clinopyroxene Fe^{2+}–Mg geothermometer: an updated calibration. J. Metamorph. Geol. 18, 211–219.
Krogh, E.J., 1988. The garnet-clinopyroxene Fe-Mg-geothermometer—a reinterpretation of existing experimental data. Contrib. Mineral. Petrol. 99, 44–48.
Li, C., van der Hilst, R.D., Engdahl, E.R., Burdick, S., 2008. A new global model for P wave speed variations in Earth's mantle. Geochem. Geophys. Geosyst. 9 (5). https://doi.org/10.1029/2007GC001806.
Liu, J., Pearson, D.G., Wang, L.H., Mather, K.A., Kjarsgaard, B.A., Schaeffer, A.J., Irvine, G.J., Kopylova, M.G., Armstrong, J.P., 2021. Plume-driven recratonization of deep continental lithospheric mantle. Nature 592. https://doi.org/10.1038/s41586-021-03395-5.
Masun, K.M.S., Smith, B.H., 2008. The Pimenta Bueno kimberlite field, Rondônia, Brasil: Tuffisitic kimberlite e transitional textures. J Volcanol. Geotherm. Res. 174, 81–89.
Matthews, K.J., Maloney, K.T., Zahirovic, S., Williams, S.E., Seton, M., Müller, R.D., 2016. Global plate boundary evolution and kinematics since the late Paleozoic. Glob. Planet. Change 146, 226–250. https://doi.org/10.1016/j.gloplacha.2016.10.002.
Melluso, L., Lustrino, M., Ruberti, E., Brotzu, P., de Barros Gomes, C., Morbidelli, L., Morra, V., Svisero, D.P., d'Amelio, F., 2008. Major-and trace-element composition of olivine, perovskite, clinopyroxene, Cr–Fe–Ti oxides, phlogopite and host kamafugites and kimberlites, Alto Paranaiba. Brazil. Can. Mineral. 46 (1), 19–40. https://doi.org/10.3749/canmin.46.1.19.
Menzies, M., Rogers, N., Tindle, A., Hawkesworth, C., 1987. Metasomatic and Enrichment Processes in the Lithospheric Peridotites, and Effect of Asthenosphere-Lithosphere Interaction. In: Menzies, M.A., Hawkesworth, C.J. (Eds.), Mantle Metasomatism. Academic Press, London, pp. 313–361.
Mišković, A., Spikings, R.A., Chew, D.M., Košler, J., Ulianov, A., Schaltegger, U., 2009. Tectonomagmatic evolution of western Amazonia: Geochemical characterization and zircon U-Pb geochronologic constraints from the Peruvian eastern cordilleran granitoids. Geol. Soc. Am. Bull. 121 (9–10), 1298–1324. https://doi.org/10.1130/B26488.1.
Nimis, P., Taylor, W.R., 2000. Single clinopyroxene thermobarometry for garnet peridotites. Part I. Calibration and testing of a Cr-in-Cpx barometer and an enstatite-in-Cpx thermometer. Contrib. Mineral. Petrol. 139, 541–554.
Nixon, P.H., 1987. Mantle Xenoliths. John Wiley & Sons, Chichester.
Nowell, G.M., Pearson, D.G., Bell, D.R., Carlson, R.W., Smith, C.B., Kempton, P.D., Noble, S.R., 2004. Hf Isotope Systematics of Kimberlites and their Megacrysts: New Constraints on their Source Regions. J. Petrol. 45 (8), 1583–1612. https://doi.org/10.1093/petrology/egh024.
Oliveros, V., Vásquez, P., Creixell, C., Lucassen, F., Ducea, M.N., Ciocca, I., González, J., Espinoza, M., Salazar, E., Coloma, F., Kasemann, S.A., 2020. Lithospheric evolution of the Pre- and Early Andean convergent margin. Chile. Gondwana Res. 80, 202–227 https://doi.org/10.10146/j.gr.2019.11.002.
Ordóñez-Carmona, O., Restrepo, J.J., Pimentel, M.M., 2006. Geochronological and isotropical review of pre-Devonian crustal basement of the Colombian Andes. J South Am. Earth Sci. 21, 372–382.
O'Reilly, S.Y., Griffin, W.L., 2013. Mantle Metasomatism. In: Harlow, D.E., Austrheim, H. (Eds.), Metasomatism and the Chemical Transformation of Rock: The Role of Fluids in Terrestrial and Extraterrestrial Processes. Springer, New York, pp. 471–534.
Paton, C., Hellstrom, J., Paul, B., Woodhead, J., Hergt, J., 2011. Iolite: Freeware for the visualisation and processing of mass spectrometric data. J. Anal. At. Spectrom. 26, 2508. https://doi.org/10.1039/c1ja10172b.
Pearson, D.G., Canil, D., Shirey, S., 2014. Mantle samples included in volcanic rocks: xenoliths and diamonds.In: Holland, H.D., Turekian, K.K. (Eds.), Treatise in Geochemistry, vol. 2, pp. 171-275.
Pinho, M.A.S.B., Chemale Júnior, F., Van Schmus, W.R., Pinho, F.E.C., 2003. U-Pb and Sm–Nd evidence for 1.76–1.77 Ga magmatism in the Moreru region, Mato Grosso, Brazil: implications for province boundaries in the SW Amazon Craton. Precambrian Res. 126, 1–25. https://doi.org/10.1016/S0301-9268(03)00126-8.
Pivin, M., Féménias, O., Demaiffe, D., 2009. Metasomatic mantle origin for Mbuji-Mayi and Kundelungu garnet and clinopyroxene megacrysts (Democratic Republic of Congo). Lithos 112, 951–960. https://doi.org/10.1016/j.lithos.2009.03.050.
Powell, R., 1985. Regression diagnostics and robust regression in geothermometer/geobarometer calibration: the garnet-clinopyroxene geothermometer revisited. J Metamorph. Geol. 3, 231–243.

Priestley, K., McKenzie, D., Ho, T., 2018. A lithosphere-asthenosphere boundary: A global model derived from multimode surface-wave tomography and petrology. In: Yuan, H., Romanowicz, B. (Eds.), Lithospheric Discontinuities. American Geophysical Union. https://doi.org/10.1002/9781119249740.ch6.

Raczek, I., Peter Jochum, K., Hofmann, A.W., 2003. Neodymium and Strontium Isotope Data for USGS Reference Materials BCR-1, BCR -2, BHV O-1, BHVO-2, AGV-1, AGV-2, GSP-1, GSP-2 and Eight MPI-DING Reference Glasses. Geostandard. Newslett. 27 (2), 173–179. https://doi.org/10.1111/j.1751-908X.2003.tb00644.x.

Read, G., Grutter, H., Winter, S., Luckman, N., Gaunt, F., Thomsen, F., 2004. Stratigraphic relations, kimberlite emplacement and lithospheric thermal evolution, Quiricó Basin, Minas Gerais State. Brazil. Lithos 77 (1–4), 803–818. https://doi.org/10.1016/j.lithos.2004.04.011.

Reitsma, M.J., 2012. Reconstructing the late Paleozoic: Early Mesozoic plutonic and sedimentary record of south–east Peru: Orphaned back–arcs along the western margin of Gondwana. Doctoral thesis, University of Geneva, 226 p. Geneva. Doi: 10.13097/archive-ouverte/unige:23095.

Restrepo, J.J., Ordóñez-Carmona, O., Armstrong, R., Pimentel, M.M., 2011. Triassic metamorphism in the northern part of the Tahamí Terrane of the central cordillera of Colombia. J. South Am. Earth Sci. 32, 497–507.

Rizzotto, G.J., Santos, J.O.S., Hartman, L.A., Tohver, E., Pimentel, M.M., McNaugthon, N.J., 2013. The Mesoproterozoic Guaporé suture in the SW Amazonian Craton: geotectonic implications based on field geology, zircon geochronology e Nd–Sr isotope geochemistry. J. South Am. Earth Sci. 48, 271–295.

Rudnick, R.L., McDonough, W.F., Chappell, B.C., 1993. Carbonatite metasomatism in the northern Tanzanian mantle. Earth Planet. Sci. Lett. 114, 463–475.

Santos, J.O.S., 2003. Geotectônica do Escudo das Guianas e Brasil-Central. In: Bizzi, L. A., Schobbenhaus, C., Vidotti, R.M., Gonçalves, J.H. (Eds.), Geologia, Tectônica e Recursos Minerais do Brasil. Brasília, CPRM, pp. 169–226.

Santos, J.O.S., Hartman, L.A., Gaudette, H.E., Groves, D.I., McNaughton, N.J., Fletcher, I.R., 2000. A new understanding of the provinces of the Amazon Craton based on integration of field mapping and U-Pb and Sm-Nd geochronology. Gondwana Res. 3 (4), 453–488.

Santos, J.O.S., Rizzotto, G.J., Potter, P., McNaughton, N., Matos, R., Hartmann, L., Chemale Jr., F., Quadros, M., 2008. Age and autochthonous evolution of the Sunsás Orogen in West Amazon Craton based on mapping and U-Pb geochronology. Precambrian Res. 165, 120–152.

Schulze, D., 2003. A classification scheme for mantle-derived garnets in kimberlite: a tool for investigating the mantle and exploring for diamonds. Lithos 71, 195–213. https://doi.org/10.1016/S0024-4937(03)00113-0.

Sgarbi, P.B., Heaman, L.M., Gaspar, J.C., 2004. U-Pb perovskite ages for brazilian kamafugitic rocks: further support for a temporal link to a mantle plume hotspot track. J. South Am. Earth Sci. 16 (8), 715–724. https://doi.org/10.1016/j.jsames.2003.12.005.

Smith, D. and Griffin, W.L., 2005. Garnetite Xenoliths and Mantle–Water Interactions Below the Colorado Plateau, Southwestern United States. J. Petrol. 46(9), 1901-1924. Doi: 10.1093/petrology/egi042.

Shu, Q., Brey, G.P., Gerdes, A., Hoefer, H.E., 2014. Mantle eclogites and garnet pyroxenites – the meaning of two-point isochrons, Sm–Nd and Lu–Hf closure temperatures and the cooling of the subcratonic mantle. Earth Planet. Sci. Lett. 389, 143–154. https://doi.org/10.1016/j.epsl.2013.12.028.

Smart, K.A., Cartigny, P., Tappe, S., O'Brien, H., Klemme, S., 2017. Lithospheric diamond formation as a consequence of methane-rich volatile flooding: An example from diamondiferous eclogite xenoliths of the Karelian craton (Finland). Geochim. Cosmochim. Acta 206, 312–342.

Spetsius, Z.V., Taylor, L.A., 2002. Partial melting in mantle eclogite xenoliths: connections with diamond paragenesis. Int. Geol. Rev. 44, 973–987. https://doi.org/10.2747/0020-6814.44.11.973.

Spikings, R. and Paul, A., 2019. The Permian–Triassic history of magmatic rocks of the northern Andes (Colombia and Ecuador): Supercontinent assembly and disassembly. In: Gómez, J., Pinilla–Pachon, A.O. (Eds.), The Geology of Colombia, Volume 2 Mesozoic. Servicio Geológico Colombiano, Publicaciones Geológicas Especiales 36, p. 1-43. Bogotá. Doi: 10.32685/pub.esp.36.2019.01.

Spikings, R., Reitsma, M.J., Boekhout, F., Mišković, A., Ulianov, A., Chiaradia, M., Gerdes, A., Schaltegger, U., 2016. Characterization of Triassic rifting in Peru and implications for the early disassembly of western Pangaea. Gondwana Res. 35, 124–143. https://doi.org/10.1016/j.gr.2016.02.008.

Su, B., Chen, Y., Guo, S., Chen, S., Li, Y.-B., 2019. Garnetite and pyroxenite in the mantle wedge formed by slab-mantle interactions at different melt/rock ratios. J. Geophy. Res.: Solid Earth 124, 6504–6522. https://doi.org/10.1029/2019JB017347.

Sun, S., McDonough, W.F., 1989. Chemical and isotopic systematics of oceanic basalts: implications for mantle composition and processes. Geol. Soc. London. Spec. Publ. 42, 313–345 http://dx.doi.10.1144/GSL.SP.1989.042.01.19.

Sweeney, R.J., Thompson, A.B., Ulmer, P., 1993. Phase relations of a natural MARID composition and implications for MARID genesis, lithospheric melting and mantle metasomatism. Contrib. Mineral. Petrol. 115, 225–241.

Tappe, S., Foley, S.F., Jenner, G.A., Heaman, L.M., Kjarsgaard, B.A., Romer, R.L., Stracke, A., Joyce, N., Hoefs, J., 2006. Genesis of ultramafic lamprophyres and carbonatites at Aillik Bay, Labrador: A consequence of incipient lithospheric thinning beneath the North Atlantic craton. J. Petrol. 47 (7), 1261–1315.

Tappe, S., Romer, R.L., Stracke, A., Steenfelt, A., Smart, K.A., Muehlenbachs, K., Torsvik, T.H., 2017. Sources and mobility of carbonate melts beneath cratons, with implications for deep carbon cycling, metasomatism and rift initiation. Earth Planet. Sci. Lett. 466, 152–167.

Tappe, S., Budde, G., Stracke, A., Wilson, A., Kleine, T., 2020. The tungsten-182 record of kimberlites above the African superplume: Exploring links to the core-mantle boundary. Earth Planet. Sci. Lett. 547, 116473. https://doi.org/10.1016/j.epsl.2020.116473.

Tappe, S., Massuyeau, M., Smart, K.A., Woodland, A.B., Gussone, N., Milne, S., Stracke, A., 2021a. Sheared peridotite and megacryst formation beneath the Kaapvaal craton: A snapshot of tectonomagmatic processes across the lithosphere–asthenosphere transition. J. Petrol. 62 (8), 1–39.

Tappe, S., Shaikh, A.M., Wilson, A.H. and Stracke, A., 2021b. Evolution of ultrapotassic volcanism on the Kaapvaal craton: deepening the orangeite versus lamproite debate. Geological Society, London, Special Publications, SP513: SP513-2021-84.

Tappe, S., Smart, K., Torsvik, T.H., Massuyeau, M., de Wit, M.C.J., 2018. Geodynamics of kimberlites on a cooling Earth: Clues to plate tectonic evolution and deep volatile cycles. Earth Planet Sci. Lett. 484, 1–14.

Thirlwall, M.F., 1991. Long-term reproducibility of multicollector Sr and Nd isotope ratio analysis. Chem. Geol. Isotope Geosci. Sect. 94 (2), 85–104. https://doi.org/10.1016/0168-9622(91)90002-E.

van der Meer, D.G., Spakman, W., van Hinsbergen, D.J.J., Amaru, M.L., Torsvik, T.H., 2010. Towards absolute plate motions constrained by lower-mantle slab remnants. Nature Geosci. 3 (1), 36–40.

van der Meer, D.G., Torsvik, T.H., Spakman, W., van Hinsbergen, D.J.J., Amaru, M.L., 2012. Intra-Panthalassa Ocean subduction zones revealed by fossil arcs and mantle structure. Nature Geosci. 5 (3), 215–219. https://doi.org/10.1038/ngeo1401.

van der Meer, D.G., van Hinsbergen, D.J.J., Spakman, W., 2018. Atlas of the underworld: Slab remnants in the mantle, their sinking history, and a new outlook on lower mantle viscosity. Tectonophysics 723, 309–448. https://doi.org/10.1016/j.tecto.2017.10.004.

Van Orman, J.A., Grove, T.L., Shimizu, N., Layne, G.D., 2002. Rare earth element diffusion in a natural pyrope single crystal at 2.8 GPa. Contrib. Mineral. Petrol. 142, 416–424.

Vinasco, C.J., Cordani, U.G., González, H., Weber, M., Peláez, C., 2006. Geochronological, isotopic, and geochemical data from Permo-Triassic granitic gneisses and granitoids of the Colombian Central Andes. J. South Am. Earth Sci. 21 (4), 355–371.

Viscarret, P., Wright, J., Urbani, F., 2009. New U-Pb zircon ages of El Baúl Massif, Cojedes state, Venezuela. Revista Técnica de la Facultad de Ingeniería, Universidad del Zulia 32(3), 210-221.

Walter M. J., 1999. Melting residues of fertile peridotite and the origin of cratonic lithosphere. In: Mantle Petrology: Field Observations and High-Pressure Experimentation. Spec. Publ. Geochem. In: Fei, Y., Bertka, C. M., Mysen, B. O. Soc. No. 6 Geochemical Society, Houston. pp. 225–239.

Wass, S., Henderson, P., Elliott, C., 1980. Chemical heterogeneity and metasomatism in the upper mantle: evidence from rare earth and other elements in apatite-rich xenoliths in basaltic rocks from eastern Australia. Phil. Trans. R. Soc. Lond. A 297, 333–346.

Waters, F.G., 1987. A suggested origin of MARID xenoliths in kimberlites by high pressure crystallization of an ultrapotassic rock such as lamproite. Contrib. Mineral. Petrol. 95, 523–533.

Weska, R.K., Barbosa, P.F., Martins, M.V.C., Souza, V.S., Dantas, E.L., 2020. Pectolite in the Carolina kimberlitic intrusion, Espigão D'Oeste – Rondônia. Brazil. J. South Am. Earth Sci. 100,. https://doi.org/10.1016/j.jsames.2020.102583 102583.

Zolinger, I.T., 2005. As intrusões de afinidade kimberlítica E1 e Es1 da região de Colorado do Oeste, Rondônia. University of São Paulo (USP), São Paulo, Brazil, p. 130. PhD thesis.